37. Lee MJ, Chen YF, Fan PC, Wang KC, Wang K, Wang J, et al. Mutation genotypes of RNF213 gene from moyamoya patients in Taiwan. J Neurol Sci. 2015;353:161–5. doi:10.1016/j.jns.2015.04.019.
38. Scott RM, Smith ER. Moyamoya disease and moyamoya syndrome. N Engl J Med. 2009;360:1226–37. doi:10.1056/NEJMra0804622.
39. Harel T, Posey JE, Graham BH, Walkiewicz M, Yang Y, Lalani SR, et al. Atypical presentation of moyamoya disease in an infant with a de novo RNF213 variant. Am J Med Genet A (online:2015.7.21), doi:10.1002/ajmg.a.37230.
40. Miyatake S, Touho H, Miyake N, Ohba C, Doi H, Saitsu H, et al. Sibling cases of moyamoya disease having homozygous and heterozygous c.14576G > A variant in RNF213 showed varying clinical course and severity. J Hum Genet. 2012;57:804–6. doi:10.1038/jhg.2012.105.
41. Koizumi A, Kobayashi H, Liu W, Fujii Y, Senevirathna ST, Nanayakkara S, et al. P.R4810K, a polymorphism of RNF213, the susceptibility gene for moyamoya disease, is associated with blood pressure. Environ Health Prev Med. 2013;18:121–9. doi:10.1007/s12199-012-0299-1.
42. Ogura T, Wilkinson AJ. AAA+ superfamily ATPases: common structure–diverse function. Genes Cells. 2001;6:575–97. doi:10.1046/j.1365-2443.2001.00447.x.
43. Geisbrecht BV, Collins CS, Reuber BE, Gould SJ. Disruption of a PEX1-PEX6 interaction is the most common cause of the neurologic disorders Zellweger syndrome, neonatal adrenoleukodystrophy, and infantile Refsum disease. Proc Natl Acad Sci USA. 1998;95:8630–5.
44. Reuber BE, Germain-Lee E, Collins CS, Morrell JC, Ameritunga R, Moser HW, et al. Mutations in PEX1 are the most common cause of peroxisome biogenesis disorders. Nat Genet. 1997;17:445–8. doi:10.1038/ng1297-445.
45. Johnson JO, Mandrioli J, Benatar M, Abramzon Y, Van Deerlin VM, Trojanowski JQ, et al. Exome sequencing reveals VCP mutations as a cause of familial ALS. Neuron. 2010;68:857–64. doi:10.1016/j.neuron.2010.11.036.
46. Abramzon Y, Johnson JO, Scholz SW, Taylor JP, Brunetti M, Calvo A, et al. Valosin-containing protein (VCP) mutations in sporadic amyotrophic lateral sclerosis. Neurobiol Aging 2012;33:2231 e2231–2231 e2236. doi:10.1016/j.neurobiolaging.2012.04.005.
47. Hoshimaru M, Takahashi JA, Kikuchi H, Nagata I, Hatanaka M. Possible roles of basic fibroblast growth factor in the pathogenesis of moyamoya disease: an immunohistochemical study. J Neurosurg. 1991;75:267–70. doi:10.3171/jns.1991.75.2.0267.
48. Hojo M, Hoshimaru M, Miyamoto S, Taki W, Nagata I, Asahi M, et al. Role of transforming growth factor-beta1 in the pathogenesis of moyamoya disease. J Neurosurg. 1998;89:623–9. doi:10.3171/jns.1998.89.4.0623.
49. Aoyagi M, Fukai N, Sakamoto H, Shinkai T, Matsushima Y, Yamamoto M, et al. Altered cellular responses to serum mitogens, including platelet-derived growth factor, in cultured smooth muscle cells derived from arteries of patients with moyamoya disease. J Cell Physiol. 1991;147:191–8. doi:10.1002/jcp.1041470202.
50. Nanba R, Kuroda S, Ishikawa T, Houkin K, Iwasaki Y. Increased expression of hepatocyte growth factor in cerebrospinal fluid and intracranial artery in moyamoya disease. Stroke. 2004;35:2837–42. doi:10.1161/01.STR.0000148237.13659.e6.
51. Maruwaka M, Yoshikawa K, Okamoto S, Araki Y, Sumitomo M, Kawamura A, et al. Biomarker research for moyamoya disease in cerebrospinal fluid using surface-enhanced laser desorption/ionization time-of-flight mass spectrometry. J Stroke Cerebrovasc Dis. 2015;24:104–11. doi:10.1016/j.jstrokecerebrovasdis.2014.07.028.
52. Ohkubo K, Sakai Y, Inoue H, Akamine S, Ishizaki Y, Matsushita Y, et al. Moyamoya disease susceptibility gene RNF213 links inflammatory and angiogenic signals in endothelial cells. Sci Rep. 2015;5:13191. doi:10.1038/srep13191.
53. Kim JH, Jung JH, Phi JH, Kang HS, Kim JE, Chae JH, et al. Decreased level and defective function of circulating endothelial progenitor cells in children with moyamoya disease. J Neurosci Res. 2010;88:510–8. doi:10.1002/jnr.22228.
54. Kim CS, Ying H, Willingham MC, Cheng SY. The pituitary tumor-transforming gene promotes angiogenesis in a mouse model of follicular thyroid cancer. Carcinogenesis. 2007;28:932–9. doi:10.1093/carcin/bgl231.
55. Arnaoutova I, George J, Kleinman HK, Benton G. The endothelial cell tube formation assay on basement membrane turns 20: state of the science and the art. Angiogenesis. 2009;12:267–74. doi:10.1007/s10456-009-9146-4.
56. Hitomi T, Habu T, Kobayashi H, Okuda H, Harada KH, Osafune K, et al. The moyamoya disease susceptibility variant RNF213 R4810K (rs112735431) induces genomic instability by mitotic abnormality. Biochem Biophys Res Commun. 2013;439:419–26. doi:10.1016/j.bbrc.2013.08.067.
57. Schirmer SH, Bot PT, Fledderus JO, van der Laan AM, Volger OL, Laufs U, et al. Blocking interferon beta stimulates vascular smooth muscle cell proliferation and arteriogenesis. J Biol Chem. 2010;285:34677–85. doi:10.1074/jbc.M110.164350.
58. Takano S, Ishikawa E, Matsuda M, Yamamoto T, Matsumura A. Interferon-beta inhibits glioma angiogenesis through downregulation of vascular endothelial growth factor and upregulation of interferon inducible protein 10. Int J Oncol. 2014;45:1837–46. doi:10.3892/ijo.2014.2620.
59. Tsipis CP, Sun X, Xu K, Lamanna JC. Hypoxia-induced angiogenesis and capillary density determination. Methods Mol Biol. 2014;1135:69–80. doi:10.1007/978-1-4939-0320-7_6.
60. Yoshioka M, Kayo T, Ikeda T, Koizumi A. A novel locus, Mody4, distal to D7Mit189 on chromosome 7 determines early-onset NIDDM in nonobese C57BL/6 (Akita) mutant mice. Diabetes. 1997;46:887–94. doi:10.2337/diab.46.5.887.
61. Sonobe S, Fujimura M, Niizuma K, Nishijima Y, Ito A, Shimizu H, et al. Temporal profile of the vascular anatomy evaluated by 9.4-T magnetic resonance angiography and histopathological analysis in mice lacking RNF213: a susceptibility gene for moyamoya disease. Brain Res. 2014;1552:64–71. doi:10.1016/j.brainres.2014.01.011.
62. Fujimura M, Sonobe S, Nishijima Y, Niizuma K, Sakata H, Kure S, et al. Genetics and biomarkers of moyamoya disease: significance of RNF213 as a susceptibility gene. J Stroke. 2014;16:65–72. doi:10.5853/jos.2014.16.2.65.
63. Kasher PR, Jenkinson EM, Briolat V, Gent D, Morrissey C, Zeef LA, et al. Characterization of samhd1 morphant zebrafish recapitulates features of the human type I interferonopathy Aicardi–Goutieres syndrome. J Immunol. 2015;194:2819–25.
64. Rehwinkel J, Maelfait J, Bridgeman A, Rigby R, Hayward B, Liberatore RA, et al. SAMHD1-dependent retroviral control and escape in mice. EMBO J. 2013;32:2454–62.
65. Crow YJ, Manel N. Aicardi–Goutieres syndrome and the type I interferonopathies. Nat Rev Immunol. 2015;15:429–40. doi:10.1038/nri3850.
66. Aquino Gondim Fde. A, Leacock RO, Subrammanian TA, Cruz-Flores S. Intracerebral hemorrhage associated with Sneddon's syndrome: is ischemia-related angiogenesis the cause? Case report and review of the literature. Neuroradiology. 2003;45:368–72. doi:10.1007/s00234-003-0990-4.
67. Carhuapoma JR, D'Olhaberriague L, Levine SR. Moyamoya syndrome associated with Sneddon's syndrome and

antiphospholipid-protein antibodies. J Stroke Cerebrovasc Dis. 1999;8:51–6. doi:10.1016/S1052-3057(99)80054-8.
68. Fierini F, Barilaro A, Giambene B, Carlucci G, Grandi V, Maio V, et al. Moyamoya in a patient with Sneddon's syndrome. Clin Neurol Neurosurg. 2015;129:34–6. doi:10.1016/j.clineuro.2014.12.001.
69. Zhou Q, Yang D, Ombrello AK, Zavialov AV, Toro C, Stone DL, et al. Early-onset stroke and vasculopathy associated with mutations in ADA2. N Engl J Med. 2014;370:911–20. doi:10.1056/NEJMoa1307361.
70. Guo DC, Papke CL, Tran-Fadulu V, Regalado ES, Avidan N, Johnson RJ, et al. Mutations in smooth muscle alpha-actin (ACTA2) cause coronary artery disease, stroke, and moyamoya disease, along with thoracic aortic disease. Am J Hum Genet. 2009;84:617–27. doi:10.1016/j.ajhg.2009.04.007.
71. Herve D, Philippi A, Belbouab R, Zerah M, Chabrier S, Collardeau-Frachon S, et al. Loss of alpha1beta1 soluble guanylate cyclase, the major nitric oxide receptor, leads to moyamoya and achalasia. Am J Hum Genet. 2014;94:385–94. doi:10.1016/j.ajhg.2014.01.018.
72. Andersson ER, Lendahl U. Therapeutic modulation of Notch signalling–are we there yet? Nat Rev Drug Discov. 2014;13:357–78. doi:10.1038/nrd4252.
73. Merkel KH, Ginsberg PL, Parker JC Jr, Post MJ. Cerebrovascular disease in sickle cell anemia: a clinical, pathological and radiological correlation. Stroke. 1978;9:45–52. doi:10.1161/01.STR.9.1.45.
74. Park HW, Oh D, Kim N, Cho HY, Moon KC, Chae JH, et al. Congenital thrombotic thrombocytopenic purpura associated with unilateral moyamoya disease. Pediatr Nephrol. 2008;23:1555–8. doi:10.1007/s00467-008-0847-5.
75. Salih M, Andeejani A, Gader A, Kolawole T, Palkar V. Moyamoya syndrome associated with protein C deficiency. Med Sci Res. 1995;23:573–5.
76. Hiyama H, Kusano R, Muragaki Y, Miura N. Moyamoya disease associated with thrombotic thrombocytopenic purpura (TTP). No Shinkei Geka. 1994;22:567–72.
77. Artoni A, Selicorni A, Passamonti SM, Lecchi A, Bucciarelli P, Cerutti M, et al. Hemostatic abnormalities in Noonan syndrome. Pediatrics. 2014;133:e1299–304. doi:10.1542/peds.2013-3251.
78. Tourdot BE, Conaway S, Niisuke K, Edelstein LC, Bray PF, Holinstat M. Mechanism of race-dependent platelet activation through the protease-activated receptor-4 and Gq signaling axis. Arterioscler Thromb Vasc Biol. 2014;34:2644–50. doi:10.1161/ATVBAHA.114.304249.
79. Lattanzio S, Santilli F, Liani R, Vazzana N, Ueland T, Di Fulvio P, et al. Circulating dickkopf-1 in diabetes mellitus: association with platelet activation and effects of improved metabolic control and low-dose aspirin. J Am Heart Assoc. 2014;3:e001000. doi:10.1161/JAHA.114.001000.
80. Lasater EA, Li F, Bessler WK, Estes ML, Vemula S, Hingtgen CM, et al. Genetic and cellular evidence of vascular inflammation in neurofibromin-deficient mice and humans. J Clin Invest. 2010;120:859–70. doi:10.1172/JCI41443.
81. Lasater EA, Bessler WK, Mead LE, Horn WE, Clapp DW, Conway SJ, et al. $Nf1^{+/-}$ mice have increased neointima formation via hyperactivation of a Gleevec sensitive molecular pathway. Hum Mol Genet. 2008;17:2336–44. doi:10.1093/hmg/ddn134.
82. Zhang J, Hu H, Palma NL, Harrison JK, Mubarak KK, Carrie RD, et al. Hypoxia-induced endothelial CX3CL1 triggers lung smooth muscle cell phenotypic switching and proliferative expansion. Am J Physiol Lung Cell Mol Physiol. 2012;303:L912–22. doi:10.1152/ajplung.00014.2012.
83. Davies MG, Hagen PO. Pathobiology of intimal hyperplasia. Br J Surg. 1994;81:1254–69.
84. George PM, Oliver E, Dorfmuller P, Dubois OD, Reed DM, Kirkby NS, et al. Evidence for the involvement of type I interferon in pulmonary arterial hypertension. Circ Res. 2014;114:677–88. doi:10.1161/CIRCRESAHA.114.302221.
85. Buckley ML, Ramji DP. The influence of dysfunctional signaling and lipid homeostasis in mediating the inflammatory responses during atherosclerosis. Biochim Biophys Acta. 2015;1852:1498–510. doi:10.1016/j.bbadis.2015.04.011.
86. Zhang SM, Zhu LH, Chen HZ, Zhang R, Zhang P, Jiang DS, et al. Interferon regulatory factor 9 is critical for neointima formation following vascular injury. Nat Commun. 2014;5:5160. doi:10.1038/ncomms6160.
87. Chong PF, Ogata R, Kobayashi H, Koizumi A, Kira R. Early onset of moyamoya syndrome in a Down syndrome patient with the genetic variant RNF213 p.R4810K. Brain Dev (online:2014.12.26), doi:10.1016/j.braindev.2014.12.006.
88. Miskinyte S, Butler MG, Herve D, Sarret C, Nicolino M, Petralia JD, et al. Loss of BRCC3 deubiquitinating enzyme leads to abnormal angiogenesis and is associated with syndromic moyamoya. Am J Hum Genet. 2011;88:718–28. doi:10.1016/j.ajhg.2011.04.017.
89. Akasaki T, Kagiyama S, Omae T, Ohya Y, Ibayashi S, Abe I, et al. Asymptomatic moyamoya disease associated with coronary and renal artery stenoses—a case report. Jpn Circ J. 1998;62:136–8. doi:10.1253/jcj.62.136.
90. Lee JH, Youn TJ, Yoon YE, Park JJ, Hong SJ, Chun EJ, et al. Coronary artery stenosis in moyamoya disease: tissue characterization by 256-slice multi-detector CT and virtual histology. Circulation. 2013;127:2063–5. doi:10.1161/CIRCULATIONAHA.112.136473.
91. Choi W, Kim YN, Kim KH. Variant angina in moyamoya disease—a correlative etiology and different presentation: a case report. J Med Case Rep. 2015;9:86. doi:10.1186/s13256-015-0537-4.
92. Nam TM, Jo KI, Yeon JY, Hong SC, Kim JS. Coronary heart disease in moyamoya disease: are they concomitant or coincidence? J Korean Med Sci. 2015;30:470–4. doi:10.3346/jkms.2015.30.4.470.
93. Ikeda E. Systemic vascular changes in spontaneous occlusion of the circle of Willis. Stroke. 1991;22:1358–62. doi:10.1161/01.STR.22.11.1358.
94. Yamada I, Himeno Y, Matsushima Y, Shibuya H. Renal artery lesions in patients with moyamoya disease: angiographic findings. Stroke. 2000;31:733–7. doi:10.1161/01.STR.31.3.733.
95. Togao O, Mihara F, Yoshiura T, Tanaka A, Kuwabara Y, Morioka T, et al. Prevalence of stenoocclusive lesions in the renal and abdominal arteries in moyamoya disease. AJR Am J Roentgenol. 2004;183:119–22. doi:10.2214/ajr.183.1.1830119.
96. Kaku Y, Morioka M, Ohmori Y, Kawano T, Kai Y, Fukuoka H, et al. Outer-diameter narrowing of the internal carotid and middle cerebral arteries in moyamoya disease detected on 3D constructive interference in steady-state MR image: is arterial constrictive remodeling a major pathogenesis? Acta Neurochir. 2012;154:2151–7. doi:10.1007/s00701-012-1472-4.
97. Takeuchi K, Shimizu K. Hypoplasia of the bilateral internal carotid arteries. No Shinkei. 1957;9:37–43 **(in Japanese)**.
98. Hamilton SJ, Friedman JM. Insights into the pathogenesis of neurofibromatosis 1 vasculopathy. Clin Genet. 2000;58:341–4. doi:10.1034/j.1399-0004.2000.580501.x.
99. Farmer JP, Khan S, Khan A, Ortenberg J, Freeman C, O'Gorman AM, et al. Neurofibromatosis type 1 and the pediatric neurosurgeon: a 20-year institutional review. Pediatr Neurosurg. 2002;37:122–36.
100. Rosser TL, Vezina G, Packer RJ. Cerebrovascular abnormalities in a population of children with neurofibromatosis type 1. Neurology. 2005;64:553–5. doi:10.1212/01.WNL.0000150544.00016.69.

101. Koss M, Scott RM, Irons MB, Smith ER, Ullrich NJ. Moyamoya syndrome associated with neurofibromatosis Type 1: perioperative and long-term outcome after surgical revascularization. J Neurosurg Pediatr. 2013;11:417–25. doi:10.3171/2012.12.PEDS12281.
102. Ganesan V, Kirkham FJ. Noonan syndrome and moyamoya. Pediatr Neurol. 1997;16:256–8. doi:10.1016/S0887-8994(97)89980-8.
103. Yamashita Y, Kusaga A, Koga Y, Nagamitsu S, Matsuishi T. Noonan syndrome, moyamoya-like vascular changes, and antiphospholipid syndrome. Pediatr Neurol. 2004;31:364–6. doi:10.1016/j.pediatrneurol.2004.05.015.
104. Shiihara T, Kato M, Mitsuhashi Y, Hayasaka K. Costello syndrome showing moyamoya-like vasculopathy. Pediatr Neurol. 2005;32:361–3. doi:10.1016/j.pediatrneurol.2004.12.010.
105. Choi JH, Oh MY, Yum MS, Lee BH, Kim GH, Yoo HW. Moyamoya syndrome in a patient with Noonan-like syndrome with loose anagen hair. Pediatr Neurol. 2015;52:352–5. doi:10.1016/j.pediatrneurol.2014.11.017.
106. Rachmel A, Zeharia A, Neuman-Levin M, Weitz R, Shamir R, Dinari G. Alagille syndrome associated with moyamoya disease. Am J Med Genet. 1989;33:89–91. doi:10.1002/ajmg.1320330112.
107. Kamath BM, Spinner NB, Emerick KM, Chudley AE, Booth C, Piccoli DA, et al. Vascular anomalies in Alagille syndrome: a significant cause of morbidity and mortality. Circulation. 2004;109:1354–8. doi:10.1161/01.CIR.0000121361.01862.A4.
108. Al Kaissi A, Bieganski T, Baranska D, Chehida FB, Gharbi H, Ghachem MB, et al. Robinow syndrome: report of two cases and review of the literature. Australas Radiol. 2007;51:83–6. doi:10.1111/j.1440-1673.2006.01668.x.
109. Qaiser R, Scott RM, Smith ER. Identification of an association between Robinow syndrome and moyamoya. Pediatr Neurosurg. 2009;45:69–72. doi:10.1159/000204907.
110. Boerkoel CF, O'Neill S, Andre JL, Benke PJ, Bogdanovic R, Bulla M, et al. Manifestations and treatment of Schimke immuno-osseous dysplasia: 14 new cases and a review of the literature. Eur J Pediatr. 2000;159:1–7.
111. Lucke T, Clewing JM, Boerkoel CF, Hartmann H, Das AM, Knauth M, et al. Cerebellar atrophy in Schimke-immuno-osseous dysplasia. Am J Med Genet A. 2007;143A:2040–5. doi:10.1002/ajmg.a.31878.
112. Rauch A, Thiel CT, Schindler D, Wick U, Crow YJ, Ekici AB, et al. Mutations in the pericentrin (PCNT) gene cause primordial dwarfism. Science. 2008;319:816–9. doi:10.1126/science.1151174.
113. Bober MB, Khan N, Kaplan J, Lewis K, Feinstein JA, Scott CI Jr, et al. Majewski osteodysplastic primordial dwarfism type II (MOPD II): expanding the vascular phenotype. Am J Med Genet A. 2010;152A:960–5. doi:10.1002/ajmg.a.33252.
114. Codd PJ, Scott RM, Smith ER. Seckel syndrome and moyamoya. J Neurosurg Pediatr. 2009;3:320–4. doi:10.3171/2008.12.PEDS08205.
115. Charuvanij A, Laothamatas J, Torcharus K, Sirivimonmas S. Moyamoya disease and protein S deficiency: a case report. Pediatr Neurol. 1997;17:171–3. doi:10.1016/S0887-8994(97)00072-6.
116. Bonduel M, Hepner M, Sciuccati G, Torres AF, Tenembaum S. Prothrombotic disorders in children with moyamoya syndrome. Stroke. 2001;32:1786–92. doi:10.1161/01.STR.32.8.1786.
117. Martin GA, Viskochil D, Bollag G, McCabe PC, Crosier WJ, Haubruck H, et al. The GAP-related domain of the neurofibromatosis type 1 gene product interacts with ras p21. Cell. 1990;63:843–9.
118. Xu GF, Lin B, Tanaka K, Dunn D, Wood D, Gesteland R, et al. The catalytic domain of the neurofibromatosis type 1 gene product stimulates ras GTPase and complements ira mutants of S. cerevisiae. Cell. 1990;63:835–41.
119. Addissie YA, Kotecha U, Hart RA, Martinez AF, Kruszka P, Muenke M. Craniosynostosis and Noonan syndrome with KRAS mutations: expanding the phenotype with a case report and review of the literature. Am J Med Genet A. 2015;. doi:10.1002/ajmg.a.37259.
120. Aoki Y, Niihori T, Kawame H, Kurosawa K, Ohashi H, Tanaka Y, et al. Germline mutations in HRAS proto-oncogene cause Costello syndrome. Nat Genet. 2005;37:1038–40. doi:10.1038/ng1641.
121. Minami Y, Oishi I, Endo M, Nishita M. Ror-family receptor tyrosine kinases in noncanonical Wnt signaling: their implications in developmental morphogenesis and human diseases. Dev Dyn. 2010;239:1–15.
122. Boerkoel CF, Takashima H, John J, Yan J, Stankiewicz P, Rosenbarker L, et al. Mutant chromatin remodeling protein SMARCAL1 causes Schimke immuno-osseous dysplasia. Nat Genet. 2002;30:215–20.
123. Yigit G, Brown KE, Kayserili H, Pohl E, Caliebe A, Zahnleiter D, et al. Mutations in CDK5RAP2 cause Seckel syndrome. Mol Genet Genom Med. 2015;. doi:10.1002/mgg3.158.
124. Wu S, Xu Z, Liang H. Sneddon's syndrome: a comprehensive review of the literature. Orphanet J Rare Dis. 2014;9:215–21.

ORIGINAL RESEARCH

American Heart Association | American Stroke Association.

# Biochemical and Functional Characterization of RNF213 (Mysterin) R4810K, a Susceptibility Mutation of Moyamoya Disease, in Angiogenesis In Vitro and In Vivo

Hatasu Kobayashi, MD, PhD;* Yoshiko Matsuda, MD;* Toshiaki Hitomi, PhD;* Hiroko Okuda, PhD; Hirotomo Shioi, BS; Tetsuya Matsuda, MD, PhD; Hirohiko Imai, PhD; Masakatsu Sone, MD, PhD; Daisuke Taura, MD, PhD; Kouji H. Harada, MPH, PhD; Toshiyuki Habu, PhD; Yasushi Takagi, MD, PhD; Susumu Miyamoto, MD, PhD; Akio Koizumi, MD, PhD

***Background***—P.R4810K of *RNF213* (mysterin: rs112735431), which is an $AAA^+$ ATPase, is the susceptibility polymorphism for moyamoya disease (MMD) in East Asians. However, the role of RNF213 R4810K in the etiology of MMD is unknown.

***Methods and Results***—To clarify the role of RNF213 in known angiogenic pathways, RNF213 expression was analyzed in endothelial cells (ECs) treated with several angiogenic and antiangiogenic factors, including interferons (IFNs). RNF213 was upregulated by IFN-β through signal transducer and activator of transcription x in the promoter and mediated antiangiogenic activity of IFN-β. RNF213 wild-type (WT) overexpression could not lower angiogenesis without IFN-β, but RNF213 R4810K overexpression could. To correlate biochemical function as ATPase and the role of RNF213 oligomer formation with antiangiogenic activity, we investigated the effects of mutations in the $AAA^+$ module. A mutation of the Walker B motif (WEQ), which stabilizes oligomerization, inhibited angiogenesis, but $AAA^+$ module deletion, which cannot initiate oligomerization, did not. Intriguingly, R4810K, similar to WEQ, decreased ATPase activity, suggesting its antiangiogenic activity through stabilizing oligomers. To confirm the antiangiogenic effect of RNF213 upregulation in vivo, vascular EC- or smooth muscle cell-specific Rnf213 R4757K (R4810K ortholog) or WT transgenic (Tg) mice were exposed to hypoxia. Cerebral angiogenesis by hypoxia was suppressed in EC-specific Rnf213 R4757K Tg mice, whereas it was not suppressed in other mice.

***Conclusions***—This study suggests the importance of inflammatory signals as environmental factors and R4810K carriers for susceptibility to cerebral hypoxia. A specific inhibitor of ATP binding to the first $AAA^+$ could be a promising therapeutic candidate for MMD. **(*J Am Heart Assoc.* 2015;4:e002146 doi: 10.1161/JAHA.115.002146)**

**Key Words:** ATPase • interferon • moyamoya disease • RNF213 • transgenic mouse

Moyamoya disease (MMD) is a cerebrovascular disease, which is characterized by progressive occlusive or stenotic lesions at the terminal portion of internal carotid arteries.[1–3] MMD is currently recognized as one of the major causes of stroke in children worldwide.[4–6] Annual prevalence and incidence of MMD in Japan were reported to be 10.5 and 0.94 per 100 000, respectively.[7]

Recently, *RNF213* (mysterin) was identified as the susceptibility gene for MMD,[8,9] and the polymorphism, p.R4810K (rs112735431: G>A; referred to in the article as RNF213 R4810K) is a founder variant that is commonly found in East Asian (Japanese, Korean, and Chinese) patients.[8] In Japan and Korea, the majority (≈80%) of MMD patients have at least 1 allele of RNF213 R4810K.[8] A much larger proportion of carriers with RNF213 R4810K develop MMD than that of wild-type (WT) subjects, even though the majority of carriers with RNF213 R4810K remain unaffected with MMD.[10] Unknown factors are considered to overlay the genetic predisposition in

*From the Departments of Health and Environmental Sciences (H.K., T. Hitomi, H.O., H.S., K.H.H., A.K.), Neurosurgery (Y.M., Y.T., S.M.), and Diabetes, Endocrinology and Nutrition (M.S., D.T.), Graduate School of Medicine, and Department of Systems Science, Graduate School of Informatics (T.M., H.I.), and Radiation Biology Center (T. Habu), Kyoto University, Kyoto, Japan; Department of Preventive Medicine, St Marianna University School of Medicine, Kawasaki, Japan (T. Hitomi).*

Accompanying Tables S1 through S3 are available at http://jaha.ahajournals.org/content/4/7/e002146/suppl/DC1.

*Dr Kobayashi, Ms Matsuda, and Dr Hitomi contributed equally to this work.

**Correspondence to:** Akio Koizumi, MD, PhD, Department of Health and Environmental Sciences, Graduate School of Medicine, Kyoto University, Konoe-cho, Yoshida, Sakyo-ku, Kyoto 606-8501, Japan. E-mail: koizumi.akio.5v@kyoto-u.ac.jp

Received May 2, 2015; accepted June 3, 2015.

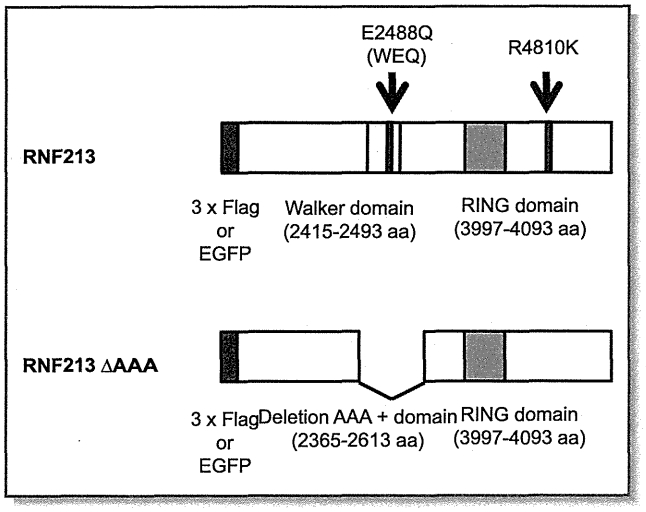


**Figure 1.** Design of tag protein (FLAG or EGFP)-RNF213 WT, RNF213 R4810K, RNF213 WEQ, and RNF213 ΔAAA vector constructs. EGFP indicates enhanced green fluorescent protein; WEQ, Walker B motif; WT, wild type.

the RNF213 R4810K carrier to develop MMD. Several case reports have suggested that MMD occurs after inflammation,[11,12] suggesting that inflammatory signals may trigger MMD as an environmental factor.

*RNF213* encodes a 591-kDa (5207 amino acids) protein that exhibits ATPase and ubiquitin ligase activities.[8] This protein was proven to be a novel $AAA^+$ ATPase, which dynamically changes its oligomeric states.[13] RNF213 has 2 $AAA^+$ ATPase modules. The first module is essential for assembling RNF213 oligomers, whereas the second module is essential to disassemble RNF213 oligomers. Both modules have Walker A and Walker B motifs and are essential for expressing ATPase activity. In the first $AAA^+$, the Walker A motif, which binds ATP, is crucial for hexamer formation, whereas the Walker B motif, which hydrolyzes and dissociates ATP, stabilizes hexamers.[13] The RNF213 R4810K variant is assembled normally as the WT,[13] suggesting that this mutation does not affect ATP binding to the Walker A motif in the first $AAA^+$.

We recently evaluated the angiogenic activity of induced pluripotent stem cell-derived vascular endothelial cells (iPSECs) from MMD patients and an unaffected carrier with RNF213 R4810K.[14] We found that angiogenic activity was lower in patients and carriers than in subjects with the WT genotype. Furthermore, the phenotype of low angiogenic activity was recaptured by overexpression of RNF213 R4810K in human umbilical vein endothelial cells (HUVECs), whereas silencing RNF213 did not alter angiogenic activity.[14,15] These observations are consistent with 2 recent independent findings in mouse models that ablation of Rnf213 did not induce any apparent abnormality of the vascular system.[16,17]

In the present study, we aimed to obtain biochemical and functional characterization of RNF213 R4810K in angiogenesis in vitro and in vivo. This aim was approached by 3 objectives. The first objective of this study was to examine whether RNF213 is a mediator in known angiogenic pathways. Therefore, we investigated angiogenic cytokines, such as vascular endothelial growth factor (VEGF), transforming growth factor (TGF)-β, platelet-derived growth factor (PDGF)-BB, and interleukin (IL)-1β,[18] as well as other antiangiogenic cytokines, including interferon (IFN)-α, IFN-β, and IFN-γ. The second objective was to investigate the effects of mutagenesis of the functional ATPase motifs in the first $AAA^+$ module on angiogenic activity. RNF213 is known to be in dynamic conformational equilibrium between oligomeric and monomeric conformations.[13] Those conformational changes of RNF213 are assumed to be related to its function. Finally, the third objective was to determine whether lower angiogenesis caused by upregulation of RNF213 R4810K in endothelial cells (ECs) can be restored in mouse models. This experiment was conducted using transgenic (Tg) mice that overexpress Rnf213 R4757K (the human R4810K allelic ortholog)

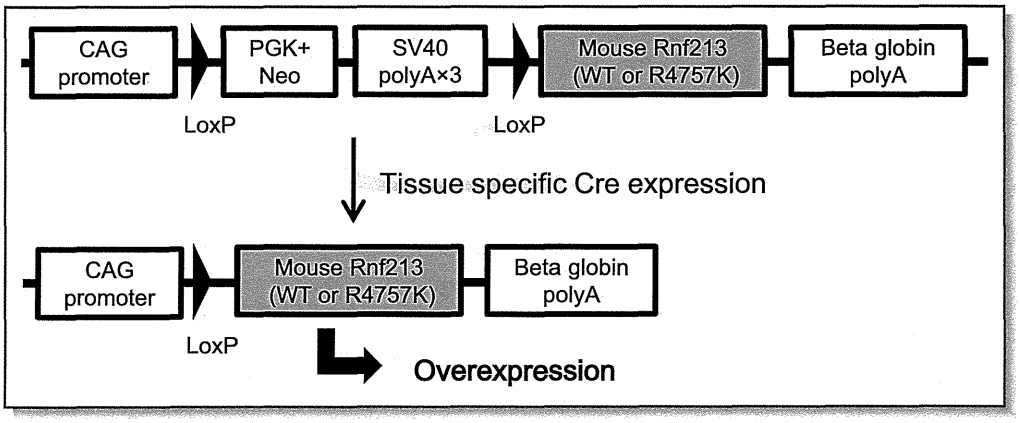


**Figure 2.** Schematic diagram of Rnf213 conditional expression in ECs or SMCs. CAG indicates cysteine-adenine-guanine; ECs, endothelial cells; SMCs, smooth muscle cells; WT, wild type.

specifically in ECs or smooth muscle cells (SMCs). Mice were exposed to hypoxia and angiogenesis was evaluated. Our results will hopefully provide further insight into RNF213 in angiogenesis.

## Methods

### Cell Culture and Reagents

HeLa cells and human embryonic kidney (HEK) 293 cells were maintained in DMEM (Invitrogen, Carlsbad, CA) containing 10% FBS (Japan Bioserum, Hiroshima, Japan). HUVECs (Lonza, Basel, Switzerland) were maintained in endothelial growth medium-2 (Lonza). iPSECs were established and maintained in primate ES medium (ReproCELL, Kanagawa, Japan), supplemented with 500 U/mL of penicillin/streptomycin (Invitrogen) and 4 ng/mL of recombinant human basic fibroblast growth factor (WAKO, Osaka, Japan), as previously reported.[14,19,20] For use and establishment of iPS cells, the institutional ethics committees of Kyoto University reviewed and approved the present study protocols. All participants gave written informed consent; for those considered too young to consent, informed consent was given by the parent or guardian.

Recombinant human IL-1β, TGF-β, VEGF, PDGF-BB, IFN-β, and IFN-γ were obtained from PeproTech (Rocky Hill, NJ). IFN-α was obtained from BioVision (Milpitas, CA). Reagents were dissolved in 0.1% BSA (GIBCO, Carlsbad, CA) at 0 ng/mL.

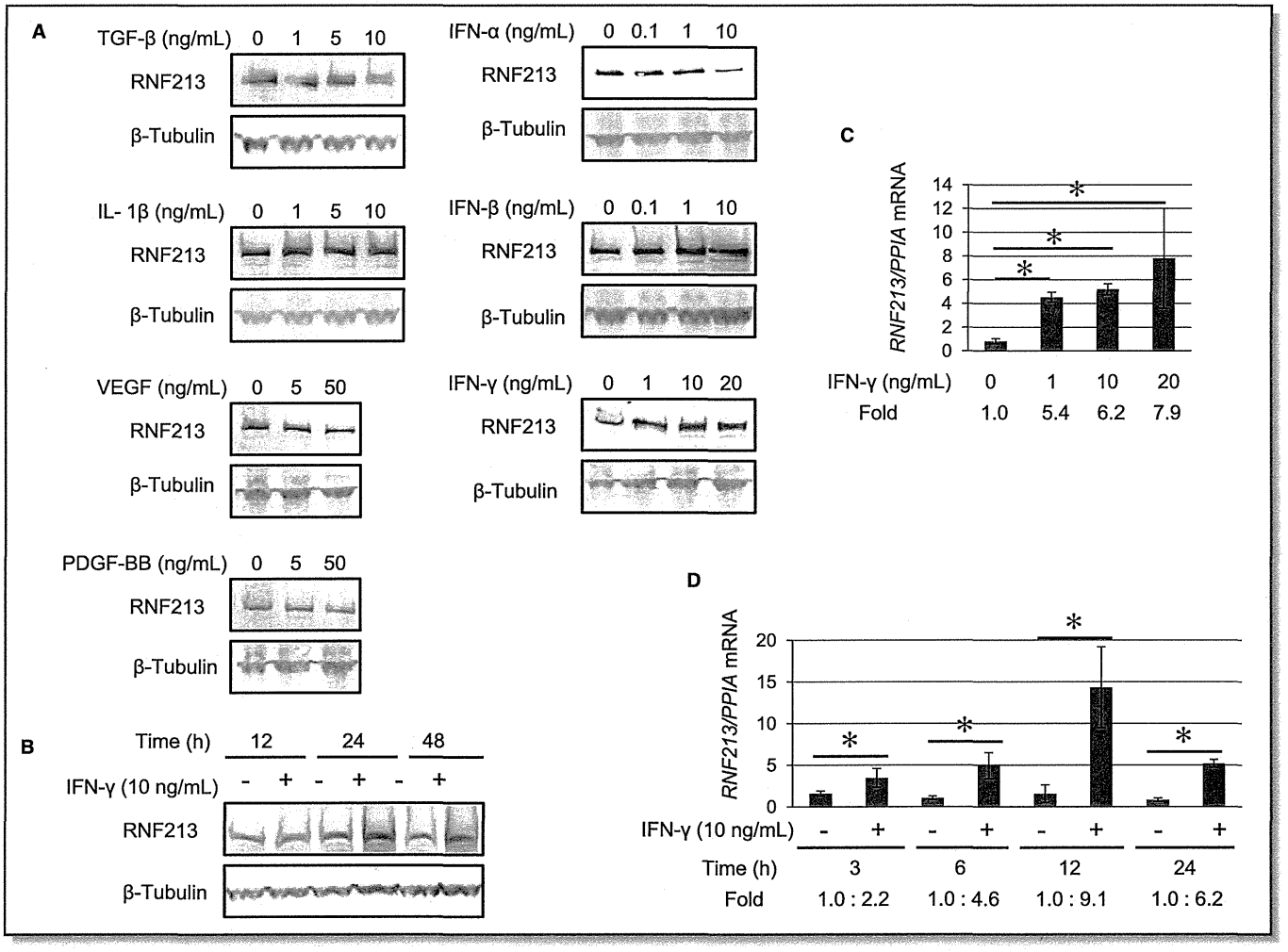


**Figure 3.** Screening the effects of angiogenic factors and antiangiogenic factors on RNF213 protein and mRNA expression in HeLa cells. A and B, HeLa cells were treated with various concentrations of angiogenic factors and antiangiogenic factors for 24 hours (A), or in the presence of 10 ng/mL of IFN-γ for the indicated times (B), and levels of RNF213 protein expression were examined by western blotting analysis using β-tubulin as a loading control. C and D, HeLa cells were treated with various concentrations of IFN-γ for 24 hours (C) or in the presence of 10 ng/mL of IFN-γ for the indicated times (D). RNA samples were analyzed by qPCR using *PPIA* as an internal control. Fold induction by IFN-γ was compared with activities of 0 ng/mL of IFN-γ. A column represents a mean of 3 independent experiments. Bars indicate SD. **P*<0.05, by Student *t* test compared with IFN-γ 0 ng/mL. IFN-γ indicates interferon γ; IL, interleukin; PDGF-BB, platelet-derived growth factor; qPCR, quantitative polymerase chain reaction; TGF-β, transforming growth factor β; VEGF, vascular endothelial growth factor.

For evaluation of cellular proliferation, HUVECs were seeded at $7.5\times10^4$ cells/well in 6-well plates. At 24 hours after seeding, the culture medium including the test reagent was exchanged. The numbers of viable cells were assessed and counted using trypan blue (Nacalai Tesque, Kyoto, Japan) exclusion.

## Evaluation of Angiogenic Activity by Tube Formation and Migration Assays

Tube formation was assessed as described previously.[14,21] HUVECs (30 000 cells/well; 0 or 1 ng/mL of IFN-β) were seeded onto 96-well plates coated with Matrigel (BD Biosciences, San Jose, CA). After incubation for 20 hours at 37°C, digital images of the tubes that formed were captured. For quantification, the area of the tube, total length of the tube, and number of tube branches were calculated using ImageJ software (National Institutes of Health, Bethesda, MD).

Migration assays were performed as described previously.[22] HUVECs were grown to overconfluence in 24-well plates and then incubated overnight for serum starvation (0 or 1 ng/mL of IFN-β). After creation of a wound with a p200 pipette tip, the medium was replaced with endothelial growth medium-2 (0 or 1 ng/mL of IFN-β). The wound was allowed to narrow for healing (re-endothelialization) for 8 hours. Digital images were obtained before and after the incubation period, and the area of re-endothelialization was calculated using ImageJ software.

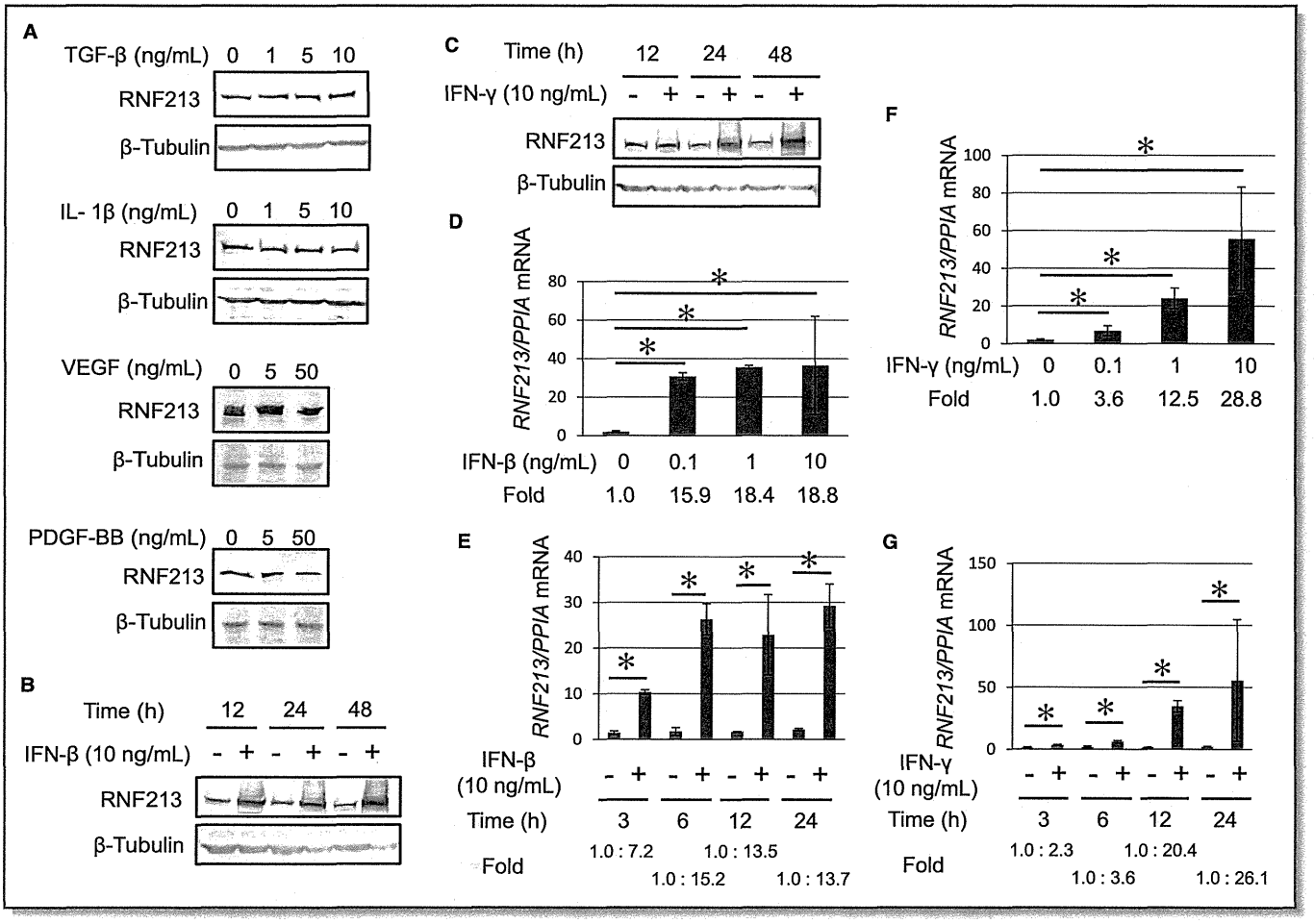


**Figure 4.** Screening effects of angiogenic factors and antiangiogenic factors on RNF213 protein and mRNA expression in HUVECs. A through C, HUVECs were treated with various concentrations of angiogenic factors for 24 hours (A), or in the presence of 10 ng/mL of IFN-β (B) or IFN-γ (C) for the indicated times, and levels of RNF213 protein expression were examined by western blotting analysis using β-tubulin as a loading control. D through G, HUVECs were treated with various concentrations of IFN-β (D) or IFN-γ (F) for 24 hours or in the presence of 10 ng/mL of IFN-β (E) or IFN-γ (G) for the indicated times. RNA samples were analyzed by qPCR using *PPIA* as an internal control. Fold induction by IFN-β or IFN-γ was compared with activities of 0 ng/mL of IFN-β or IFN-γ. A column represents a mean of 3 independent experiments. Bars indicate SD. **P*<0.05, by Student *t* test compared with 0 ng/mL IFN-β or IFN-γ. HUVECs indicates human umbilical vein endothelial cells; IFN, interferon; IL, interleukin; PDGF-BB, platelet-derived growth factor; qPCR, quantitative polymerase chain reaction; TGF-β, transforming growth factor β; VEGF, vascular endothelial growth factor.

## RNA Interference

Transfection of siRNAs was conducted using the Amaxa Nucleofector Device (Lonza), by following the manufacturer's recommendations, as previously reported.[14] We purchased and used RNF213 siRNA (sc-94184; Santa Cruz Biotechnology, Santa Cruz, CA), signal transducer and activator of transcription (STAT)1 siRNA (sc-44123; Santa Cruz Biotechnology), and control siRNA-A (sc-37007; Santa Cruz Biotechnology). Western blotting assays were conducted to monitor knockdown of gene expression.

## Plasmid Construction for RNF213 WT, RNF213 R4810K, RNF213 WEQ, and RNF213 Deletion of AAA$^+$ and Transfection

To obtain RNF213 cDNA, reverse-transcriptase polymerase chain reaction (RT-PCR) was performed using 3 sets of primers (Primer N1 to N2, M1 to M2, and C1 to C2), as shown in Table S1. We used RevTra Ace reverse transcriptase and KOD FX DNA polymerase (TOYOBO, Osaka, Japan). The 3 amplified fragments were digested with restriction enzymes (NcoI and SalI, SalI and HindIII, and HindIII and NotI, respectively). Fragments were cloned between NcoI and NotI sites of pENTR4 (Thermo Scientific, Waltham, MA) to construct full-length cDNA of RNF213. The R4810K mutation and Walker B mutation (E2488Q:WEQ) were introduced by PCR-based, site-directed mutagenesis using mutated primers using Pfu Turbo DNA polymerase (Agilent Technologies, Santa Clara, CA). These mutated primers (Primers 1 to 4) were shown in Table S1. The deleted mutation (delta AAA) was introduced by the SalI site at the 8310-nucleotide position from the start codon (primer delatSalI: AAT GTC GAC GTG ATC ACA GAA GTC CTC TGC and primer M2) by PCR using KOD FX DNA polymerase and combined with RNF213 cDNA. These entry clones were used for the LR reaction (Thermo Scientific) using a destination vector with an amino-terminal 3xFLAG tagged or enhanced green fluorescent protein (EGFP) sequence under a tetracycline-regulated cytomegalovirus promoter. The design of the tagged-RNF213 WT and mutant vectors that were used in the present study are shown in Figure 1. The generated constructs were confirmed by sequencing. The plasmids were transfected into cells using an Amaxa Nucleofector Device (Lonza), following the manufacturer's recommendations, as previously reported.[14]

## Construction of the Promoter, Transfection, and the Luciferase Assay

A DNA fragment of the human *RNF213* gene promoter, including −3000 to +200 base pairs (bp) from the transcription start site (chr17: 75 846 262 to 75 849 462 from NCBI 36/hg18), was synthesized by Takara Bio Inc (Shiga, Japan). This fragment was inserted between the *Kpn* I and *Nhe* I sites in front of the luciferase reporter gene in the pGL 4.14 Luc/Hygro vector (Promega, Madison, WI) and used as the *RNF213* WT promoter pGL4.14. The generated construct was confirmed by sequencing. A reporter plasmid with a mutation in the STATx-binding site (potential STAT1-binding) at −514/−505

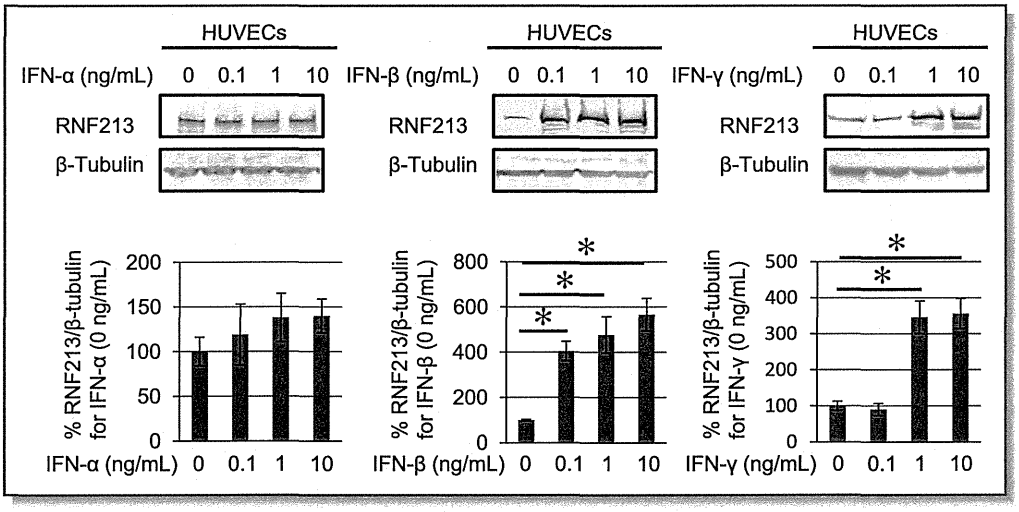


**Figure 5.** Effects of IFNs on RNF213 protein expression in HUVECs. HUVECs were treated with various concentrations of IFNs for 24 hours, and RNF213 protein expression was examined by western blotting analysis using β-tubulin as a loading control. Representative western blotting findings are shown in upper panel. A column represents a mean of 3 independent experiments (lower panel). Bars indicate SD. *$P$<0.05, by Student $t$ test compared with 0 ng/mL IFNs. HUVECs indicates human umbilical vein endothelial cells; IFNs, interferons.

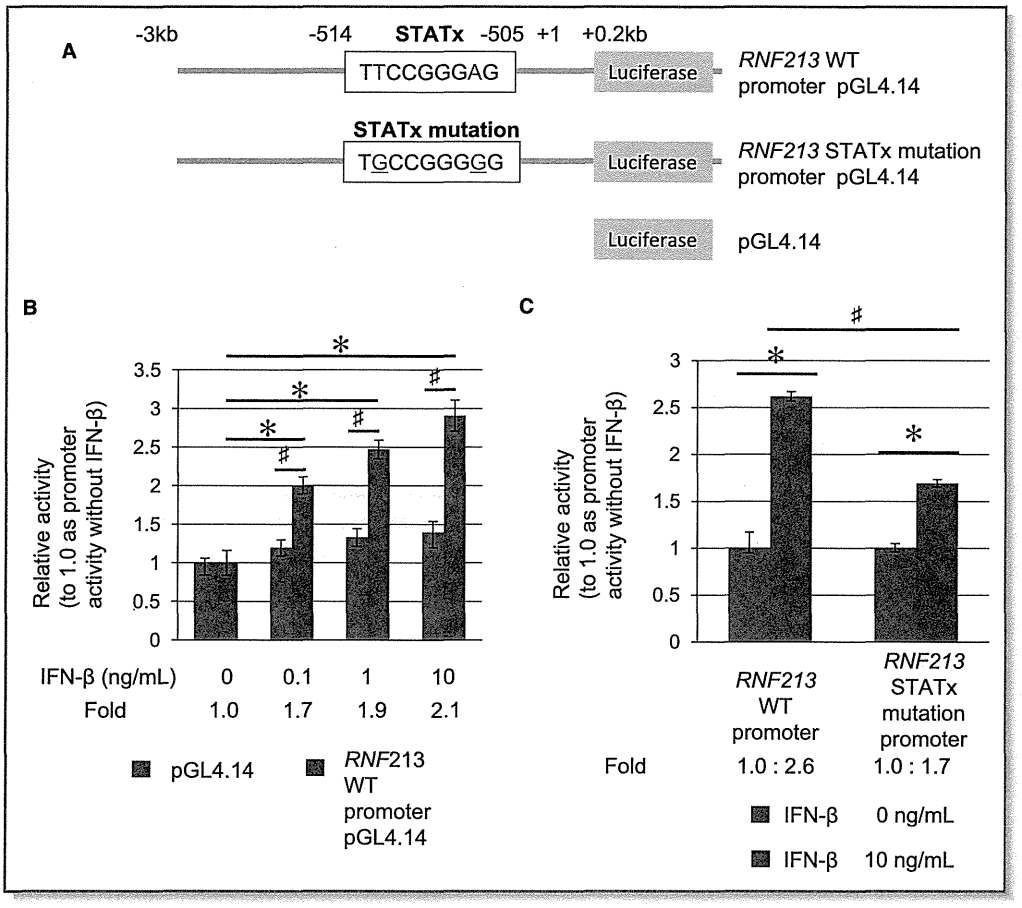


**Figure 6.** Activation of *RNF213* promoter activity in HUVECs after IFN-β treatment. A, Constructs for the *RNF213* gene promoter-luciferase fusion plasmids and the sequences of the STATx-binding site (potential STATx1-binding site; WT or mutant). Mutated nucleotides are underlined. B, Dose-response effects of IFN-β on *RNF213* gene promoter activity. Each column with a bar represents mean±SD of 3 independent experiments. Blue columns represent pGL4.14 vector. Red columns represent *RNF213* WT promoter pGL4.14 vector. Fold represents relative mean luciferase activity of *RNF213* WT promoter pGL4.14 to PGL4.14. **P*<0.05, luciferase activity at 0.1, 1, or 10 ng/mL of IFN-β were compared with 0 ng/mL of IFN-β in cells transfected with *RNF213* WT promoter pGL4.14 (red) by Student *t* test. #*P*<0.05 luciferase activity in cells transfected with *RNF213* WT promoter pGL4.14 (red) was compared with cells transfected with pGL4.14 (blue) at the same IFN-β dose by Student *t* test. C, Mutation analysis of *RNF213* gene promoter activity in HUVECs. HUVECs were transiently transfected with the *RNF213* WT promoter pGL4.14 plasmid or *RNF213* STATx mutation promoter pGL4.14 plasmid, and luciferase activities were measured after 24 hours of IFN-β treatment. Fold inductions by 10 ng/mL of IFN-β (red) were compared with the activities of IFN-β 0 ng/mL (blue). Each column with a bar represents mean±SD of 3 independent experiments. **P*<0.05, by Student *t* test compared with 0 ng/mL of IFN-β with the same promoter. #*P*<0.05 by Student *t* test compared between *RNF213* WT promoter and mutation promoter at 10 ng/mL of IFN-β. HUVECs indicates human umbilical vein endothelial cells; IFN, interferon; WT, wild type.

(5′-TGCCGGGGG-3′, mutated positions are underlined), including the *Not* I and *Sph* I sites in the *RNF213* promoter, was generated by GenScript Corp (Piscataway, NJ). The fragment was inserted between the *Not* I and *Sph* I sites in the *RNF213* WT promoter pGL4.14 plasmid construct and used as the *RNF213* STATx mutation promoter pGL4.14.

The reporter and internal control vector pGL4.74 (Promega) plasmids were transfected into cells using the Amaxa Nucleofector Device (Lonza), by following the manufacturer's recommendations, as previously reported.[14] IFN-β was added after 24 hours, and cells were harvested at 48 hours post-transfection. Luciferase activity of cell lysates was measured using the Dual-luciferase Reporter Assay System (Promega). Results were normalized by pGL4.74 luciferase activity, and the obtained values were divided by the mean value for 0 ng/mL of IFN-β.

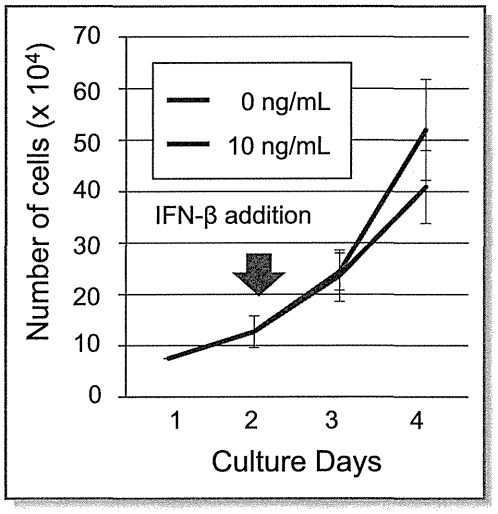


**Figure 7.** Effects of IFN-β on HUVEC proliferation as evaluated by trypan blue dye exclusion tests. At 1 day after HUVEC seeding, 0 or 10 ng/mL of IFN-β was added. Data with bars represent mean±SD (n=3). No significant difference ($P$<0.05) between 0 ng/mL of IFN-β (blue line) and 10 ng/mL of IFN-β (red line) was observed at each time point according to Student $t$ test. HUVEC indicates human umbilical vein endothelial cell; IFN, interferon.

## Biochemical Assays

Real-time quantitative PCR (qPCR) and western blotting were used as biochemical assays to assess mRNA and protein expression, respectively. qPCR was performed as described previously.[8] Target cDNA expression levels were normalized to corresponding expression levels of *PPIA*. The primer pairs that were used were as described previously.[8,14]

Western blotting was performed as described previously.[15] Lysates were subjected to immunoblotting using an anti-RNF213 antibody that we previously generated[14] or anti-STAT1 (sc-346; Santa Cruz Biotechnology), anti-FLAG (NU01102; Nacalai Tesque), anti-phospho-STAT1 (Ser727; #8826; Cell Signaling Technology, Beverly, MA), and anti-β-tubulin (sc-9104; Santa Cruz Biotechnology) antibodies. Quantification was conducted using Scion Image software (Scion Corp, Frederick, MD).

## ATPase Assay

RNF213 proteins fused with EGFP were expressed in HEK293 cells, and cells were extracted with RIPA buffer. The cell extract was clarified by high-speed centrifugation and used for immunoprecipitation with anti-GFP agarose (MBL Japan, Nagoya, Japan). Immunoprecipitants were washed with RIPA buffer twice and with RIPA buffer without SDS once, and finally equilibrated with 0.5× kinase buffer (10 mmol/L of Tris-HCl [pH 7.6], 100 mmol/L of KCl, 5 mmol/L of $MgCl_2$, and 0.025% TritonX-100). Immunoprecipitants were resuspended into 50 μL of kinase buffer, and half of this volume was subjected to SDS-PAGE and stained with GelCode staining (Thermo Scientific). To perform ATPase reactions, the indicated volume of immunoprecipitants was combined with prewarmed 1× kinase buffer with 60 μmol/L of ATP. The 50-μL ATPase reaction proceeded for 30 minutes at room temperature by adding a final concentration of Phosphate Sensor (0.5 μmol/L; Thermo Scientific). The plate was mixed and immediately read on a microplate reader at an excitation of 430 nm and emission of 450 nm.

## Vascular EC- or SMC-Specific *Rnf213* Tg Mouse Production

The transgene construct consisted of the following components: cysteine-adenine-guanine (CAG) promoter–LoxP–PGK promoter–Neo–3 SV40 poly(A) sequences–LoxP–mouse *Rnf213* (WT or R4757K mutant) coding sequence–beta globin polyA (Figure 2). The construct was generated using Gateway technology (Invitrogen). An entry vector harboring mouse Rnf213 WT was produced based on the pENTR4 vector. Five fragments of the Rnf213 coding sequence were amplified by RT-PCR from C57BL/6 mouse liver RNA using the SuperScript III One-Step RT-PCR System with Platinum Taq DNA Polymerase (Invitrogen) using primers, which are shown in Table S2. Fragments 1 and 2 were connected using the XhoI site at 3259 to 3264 bp. Fragments 2 and 3 were connected using the EcoRI site at 6080 to 6085 bp. Fragments 3 and 4 were connected using the SacII site at 8975 to 8980 bp. Fragments 4 and 5 were connected using the MluI site at 12 651 to 12 656 bp. The full-length Rnf213 coding sequence was integrated into the pENTR4 vector using NcoI and NotI sites. An allelic ortholog of human p.R4810K (p.R4757K) was introduced into *Rnf213* WT using a site-directed mutagenesis kit (Invitrogen). A donation vector was generated based on the PGKneotpAlox2 vector, containing the LoxP–PGK promoter–Neo-3 SV40 poly(A)–LoxP cassette. The CAG promoter and beta-globin polyA were amplified using the pCAGGS vector as a template. The Gateway recombination cassette (attR1-ccdB-attR2) was amplified using the pDEST vector as a template. The CAG promoter was cloned into the PGKneotpAlox2 vector, upstream of the first LoxP using SacI and NotI sites. The AttR1-ccdB-attR2 cassette and beta-globin polyA were introduced into the PGKneotpAlox2 vector, downstream of the second LoxP using NheI and XhoI sites and XhoI and KpnI sites, respectively. The entry and donation vectors were converted by an LR plus clonase reaction to produce the transgene construct.

The transgene constructs were digested with PvuI and KpnI, and a DNA fragment of 20 kb was purified and then microinjected into fertilized C57BL/6 mouse eggs to generate Tg mice. Genotypes of Tg offspring were determined by PCR using the

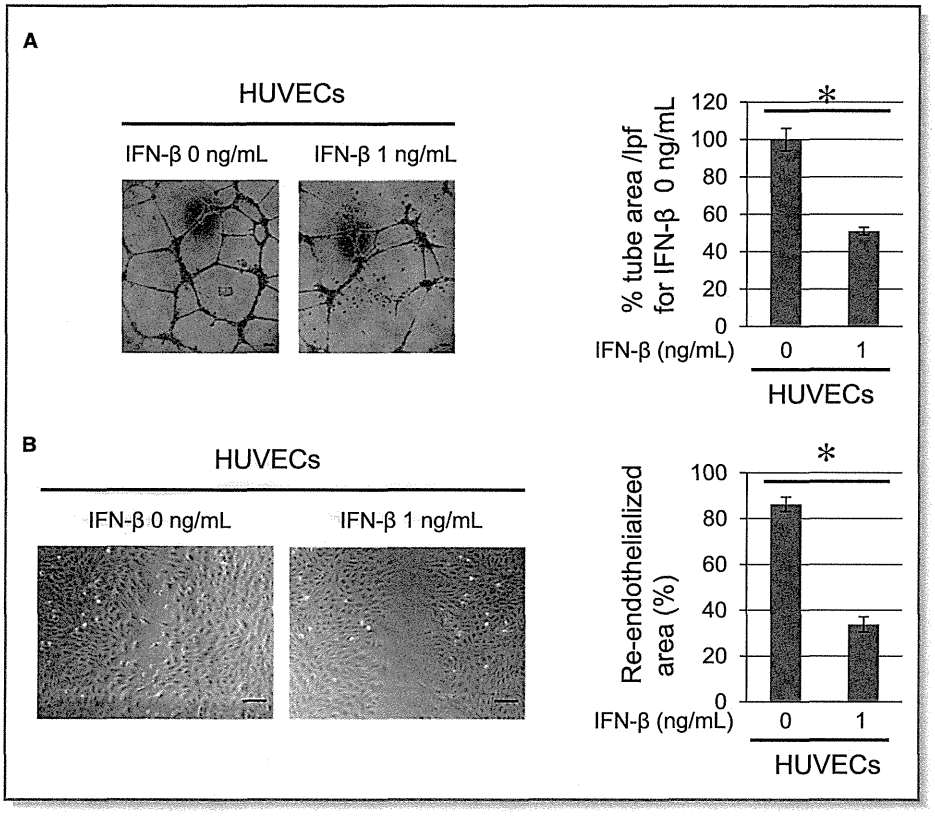


**Figure 8.** Antiangiogenic activity of IFN-β in HUVECs. A, Tube formation assays in HUVECs after 20 hours of culture with IFN-β on Matrigel. A concentration of 0 ng/mL of IFN-β was used as a positive control (100%). Scale bars indicate 100 μm. Representative images are shown in left panel. The tubal areas were quantified by imaging analysis (right panel). Data with bars represent mean±SD (n=3). **P*<0.05 according to Student *t* test compared with 0 ng/mL of IFN-β. B, Migration assays for HUVECs after treatment with IFN-β (1 ng/mL). A concentration of 0 ng/mL of IFN-β was used as a control. Scale bars indicate 100 μm. Representative images are shown in left panel. Re-endothelialized areas were quantified by imaging analysis (right panel). Data with bars represent mean±SD (n=3). **P*<0.05 according to Student *t* test compared with 0 ng/mL of IFN-β. HUVECs indicates human umbilical vein endothelial cells; IFN, interferon.

primers shown in Table S3. To obtain mice harboring vascular ECs or SMCs overexpressing Rnf213, Tg founders were bred with mice expressing a Cre transgene driven by either the Tie2 kinase promoter/enhancer (Tek; strain name: B6.Cg-Tg(Tek-cre)12Flv/J) or the smooth muscle protein 22-alpha promoter (strain name: B6.Cg-Tg(Tagln-cre)1Her/J; The Jackson Laboratory, Bar Harbor, ME). Specific expression in ECs or SMCs was confirmed by western blotting. ECs were purified from lungs by magnetic cell sorting using anti-CD31/PECAM-1 antibody (Life Technology, Grand Island, NY). Aorta was used as an SMC source.

## Exposure to Hypoxia and Evaluation of Cerebral Angiogenesis

Hypoxia experiments were performed in 5 groups of 3-week-old mice: (1) vascular EC-specific Rnf213 R4757K Tg mice (EC-Mut Tg); (2) vascular EC-specific WT Rnf213 Tg mice (EC-WT Tg); (3) vascular SMC-specific Rnf213 R4757K Tg mice

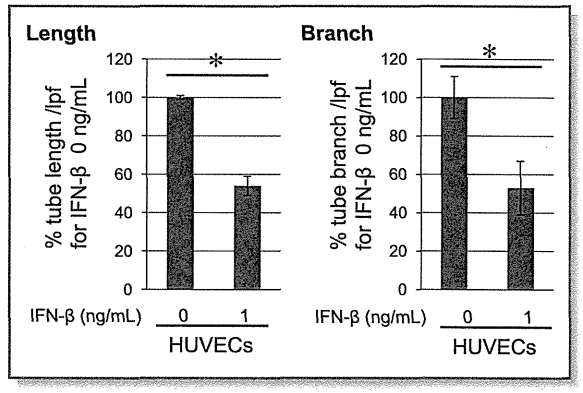


**Figure 9.** Tube formation by HUVECs after 20 hours of culture on Matrigel with IFN-β. IFN-β (0 ng/mL) served as the positive control (100%). Total tube length and number of branches were quantified by imaging analysis. Data with bars represent mean±SD (n=3). **P*<0.05 according to Student *t* test compared with 0 ng/mL of IFN-β. HUVECs indicates human umbilical vein endothelial cells; IFN, interferon.

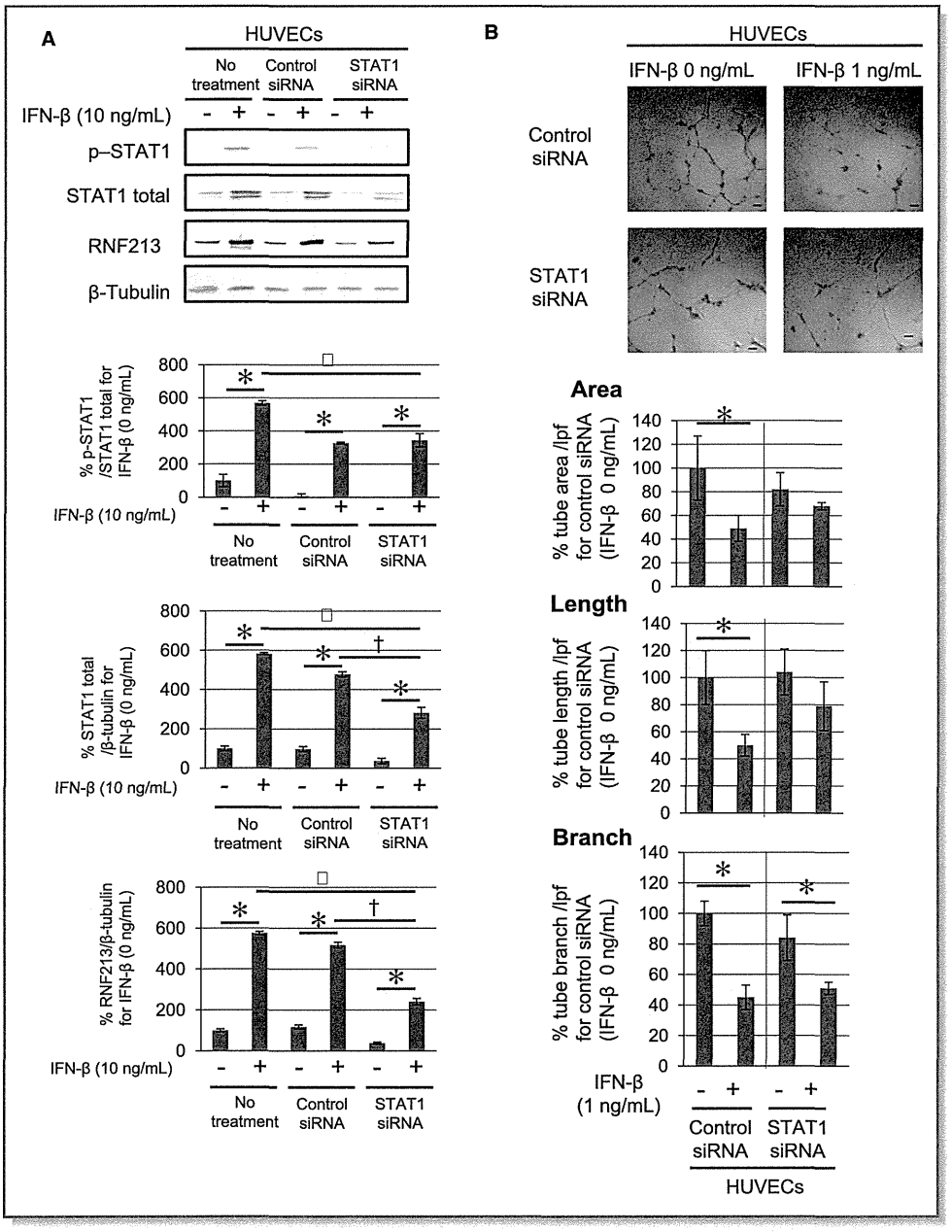


**Figure 10.** Effects of STAT1 depletion on RNF213 expression and antiangiogenic activities of IFN-β in HUVECs. A, Western blot analyses of RNF213 and STAT1 protein expressions and STAT1 protein phosphorylation (at Ser727; p-STAT1) in HUVECs treated with IFN-β for 24 hours after control or STAT1 siRNA transfection. β-tubulin served as the loading control. Representative western blot experiments are shown in the upper panel. A column with a bar (lower panel) represents mean±SD (n=3). **P*<0.05 according to Student *t* test compared with 0 ng/mL of IFN-β with the same siRNA treatment. #*P*<0.05, cells treated with 10 ng/mL of IFN-β were compared between STAT1 siRNA treatment and no siRNA treatment using Student *t* test. †*P*<0.05, STAT1 siRNA treatment was compared with control siRNA at 10 ng/mL of IFN-β using Student *t* test. B, Tube formation assays for HUVECs cultured with IFN-β on Matrigel after control or STAT1 siRNA transfection. Treatment with 0 ng/mL of IFN-β after control siRNA transfection was evaluated as a positive control (100%). Scale bars indicate 100 μm. Representative images are shown in upper panel. The tube area, total tube length, and number of branches were quantified by imaging analysis (lower panel). A column with a bar represents mean±SD (n=3). **P*<0.05, according to Student *t* test comparing 0 ng/mL of IFN-β within the same siRNA treatment paradigm. HUVECs indicates human umbilical vein endothelial cells; IFN, interferon; p-STAT1, phosphorylated signal transducer and activator of transduction 1.

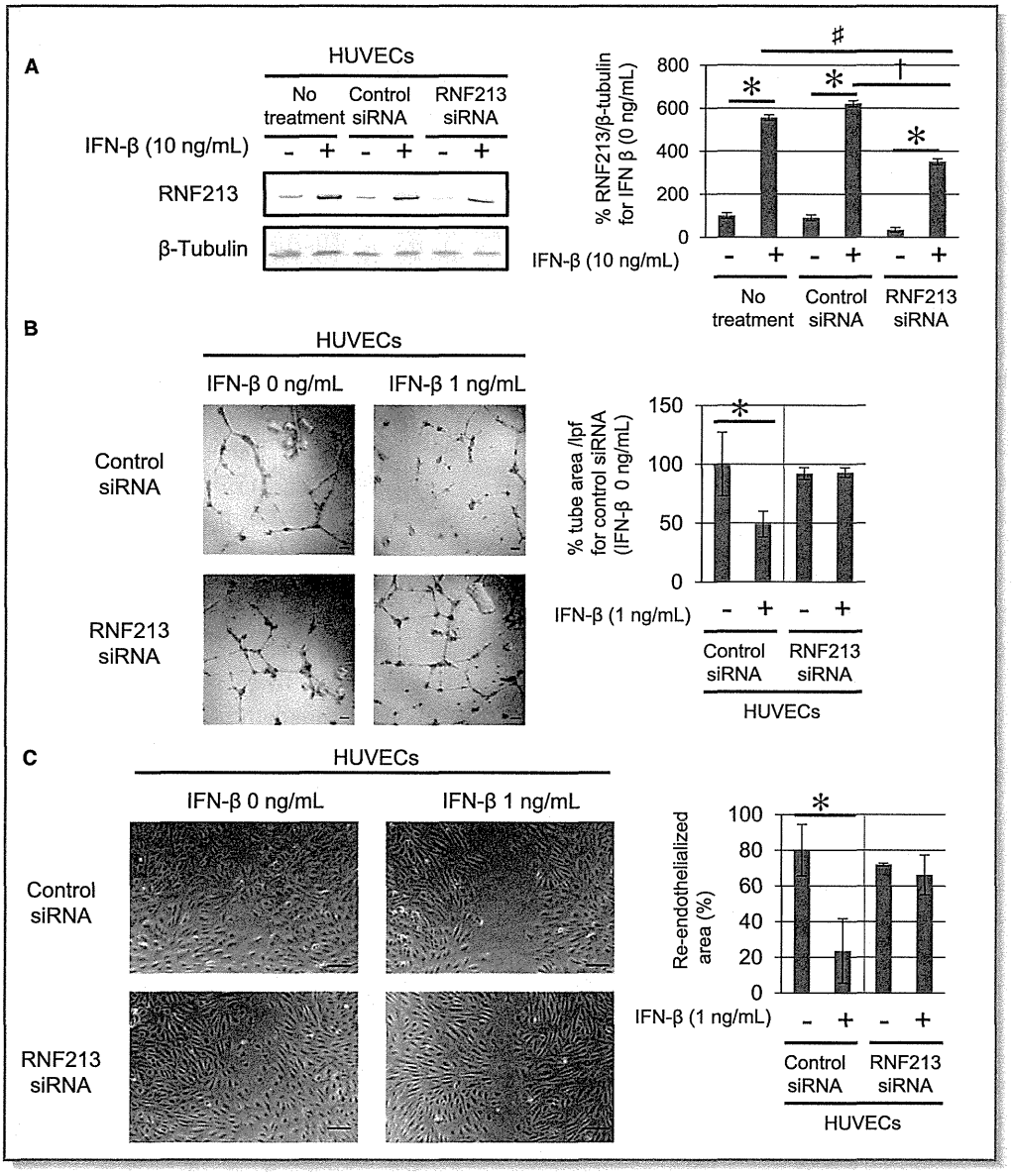


**Figure 11.** Effects of RNF213 depletion on antiangiogenic activity of IFN-β in HUVECs. A, Western blot analysis of RNF213 protein expression in HUVECs treated with IFN-β for 24 hours after control or RNF213 siRNA transfection. β-tubulin served as the loading control. Representative western blotting results are shown in left panel. A column with a bar (right panel) represents mean±SD (n=3). **P*<0.05, according to Student *t* test comparing 0 ng/mL of IFN-β within the same siRNA treatment paradigm. #*P*<0.05, cells exposed to 10 ng/mL of IFN-β were compared between RNF213 siRNA treatment and no treatment using Student *t* test. †*P*<0.05, using Student *t* test comparing control siRNA at 10 ng/mL of IFN-β. B, Tube formation assays for HUVECs cultured with IFN-β on Matrigel after control or RNF213 siRNA transfection. Treatment with 0 ng/mL of IFN-β after control siRNA transfection was used as a positive control (100%). Scale bars indicate 100 μm. Representative images are shown in left panel. Tube area was quantified by imaging analysis (right panel). A column with a bar represents mean±SD (n=3). **P*<0.05, according to Student *t* test comparing 0 ng/mL of IFN-β within the same siRNA treatment paradigm. C, Migration assays for HUVECs treated with IFN-β (1 ng/mL) after control or RNF213 siRNA transfection. Treatment with 0 ng/mL of IFN-β after control siRNA transfection served as the control. Scale bars indicate 100 μm. Representative images are shown in left panel. Re-endothelialized areas were quantified by imaging analysis (right panel). A column with a bar represents mean±SD (n=3). **P*<0.05, according to Student *t* test comparing 0 ng/mL of IFN-β within the same siRNA treatment paradigm. HUVECs indicates human umbilical vein endothelial cells; IFN, interferon.

(SMC-Mut Tg); (4) Rnf213 knockout (KO) mice[17]; and (5) WT mice. Each group was composed of mice with hypoxia (n=6) and with normoxia (n=6). Care of animals and all experimental procedures were in accord with the Animal Welfare Guidelines of Kyoto University (Kyoto, Japan), and animal protocols were reviewed and approved by the animal care, use and ethics committee at Kyoto University. Mice that were exposed to hypoxia were placed in an 8% oxygen chamber with nitrogen-balanced gas under normal-pressure atmosphere (Kyodo International, Kanagawa, Japan) for 2 weeks.

Hypoxia-induced cerebral angiogenesis was evaluated by staining for the blood–brain barrier using glucose transporter (GLUT)-1 immunohistochemistry.[23] After hypoxic exposure, mice were anesthetized and perfused with PBS with 1 U/mL of heparin. Brains were removed, fixed in 10% formaldehyde, embedded in paraffin, and sectioned. Sections were immunostained with mouse anti-Glut1 antibody (Abcam, Cambridge, MA). We captured images at ×200 magnification in the cerebral cortex from each of the 2 sections in 6 mice per genotype in hypoxia or normoxia and counted Glut1-positive capillaries using ImageJ software.

## Magnetic Resonance Imaging

Magnetic resonance angiography (MRA) was performed using a 7-T Bruker MRI (Bruker Biospin, Rheinstetten, Germany). Mice were anesthetized by inhalation of 3% isoflurane in room air, and the respiratory rate was continuously monitored. Core temperature was maintained at 30±2°C by a flow of warm air. A 3-dimensional (3D) gradient-echo sequence was used to acquire MRA images with the following parameters: field of view (FOV)=19.2×12.8×9.6 mm; matrix=192×128×96; repetition time/echo time (TR/TE)=120/4.3 ms; flip angle=60 degrees, and scan time=1 hour, 39 minutes.

To detect infarction, T2-weighted images were also acquired using a rapid acquisition with relaxation enhancement sequence with the following parameters: TE/TR=5000/15 ms; effective TE=60 ms; echo train length=8; FOV=19.2×19.2 $mm^2$; slice thickness=0.6 mm; matrix=256×256; and the number of excitations=4.

## Statistical Analysis

Results are presented as mean±SD. Number of samples are provided in the figure legends. Statistical tests on in vitro experiments were performed using the Student *t* test to detect the effect of treatments by comparing controls according to study designs shown below.

We first screened several angiogenic and antiangiogenic cytokines to determine whether treatment with different doses of these cytokines induced RNF213 in cultured cells. IFN-β and IFN-γ were found to induce RNF213. We then statistically compared RNF213 levels in IFN-β- or IFN-γ-treated cells with untreated cells. The mechanism of RNF213 induction with IFN-β was examined in cells transfected with RNF213 WT or mutated promoter luciferase plasmid. To test the effect of a STATx mutation, luciferase activity in cells transfected with STATx mutation promoter was compared with cells transfected with RNF213 WT promoter. Effects of treatment of IFN-β on angiogenesis were statistically evaluated by tube formation and migration assay using HUVECs and iPSECs. In experiments of target protein depletion (p-STAT1, STAT1, or RNF213) using corresponding siRNAs, we compared target protein levels in cells treated with target siRNA with cells treated with control siRNA. We also tested the effect of STAT1 and RNF213 siRNA on angiogenesis.

To evaluate the in vitro effect of various RNF213 mutations on angiogenesis, the angiogenic function of HUVECs transfected with RNF213 mutants were compared with HUVECs transfected with a control vector. In addition, ATPase activities of RNF213 mutants were compared to RNF213 WT.

For in vivo animal studies, both nonparametric methods (Kruskal–Wallis 1-way ANOVA followed by Mann–Whitney *U* test) and a parametric method (2-way ANOVA method) were conducted to detect effects of treatment (hypoxia), genotype, and interaction on cerebral angiogenesis. Cerebral angiogenesis was evaluated by the increase in the numbers of cerebral microvessels/$mm^2$.

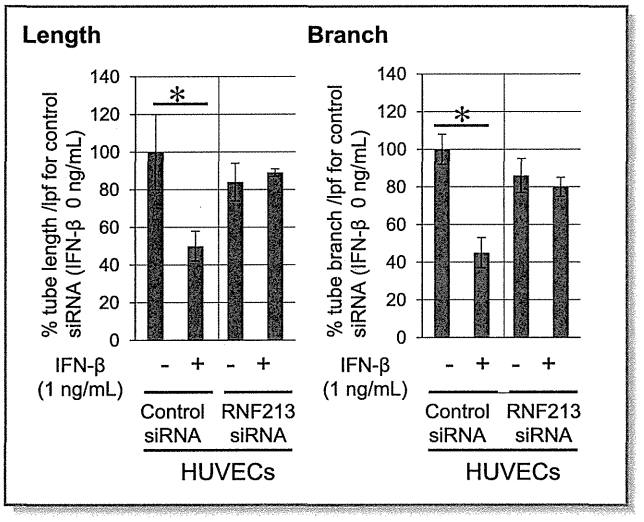


**Figure 12.** Tube formation assays for HUVECs after 20 hours of culture on Matrigel with IFN-β after control or RNF213 siRNA transfection. Treatment with 0 ng/mL of IFN-β after control siRNA transfection served as the positive control (100%). Total tube length and number of branches were quantified by imaging analysis. A column with a bar represents means±SD (n=3). **P<0.05, by Student t test compared with 0 ng/mL of IFN-β* within the same siRNA treatment. HUVECs indicates human umbilical vein endothelial cells; IFN, interferon; iPSECs, induced pluripotent stem cell-derived vascular endothelial cells.

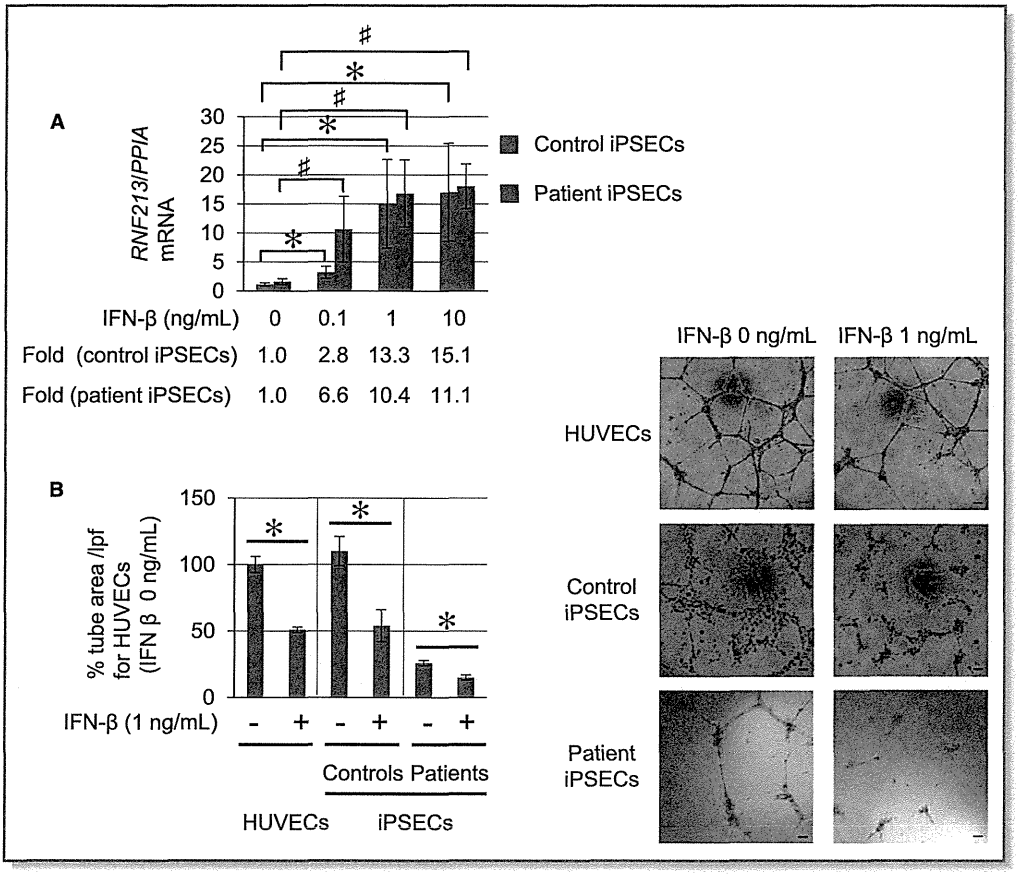


**Figure 13.** Effects of IFN-β on RNF213 protein expression and antiangiogenic activity in iPSECs from control subjects (GG genotype) and MMD patients (AA genotype). A, RNF213 mRNA levels in iPSECs treated with IFN-β for 24 hours. Fold induction attributed to IFN-β was compared with activity at 0 ng/mL of IFN-β. A column with a bar represents mean±SD of 2 controls (blue) or 2 patients (red) in 3 independent experiments. **P*<0.05, according to Student *t* test comparing 0 ng/mL of IFN-β in control (blue) iPSECs at 0.1, 1, or 10 ng/mL. #*P*<0.05, according to Student *t* test comparing 0 ng/mL of IFN-β in patient (red) iPSECs at 0.1, 1, or 10 ng/mL. B, Representative photomicrographs (right panel) and quantified tubal area (left panel) of HUVECs and iPSECs treated with IFN-β. Scale bars indicate 100 μm. HUVECs without IFN-β treatment served as the positive control (100%). A column with a bar represents mean±SD of 2 controls or 2 patients in 3 independent experiments. **P*<0.05 according to Student *t* test comparing 0 ng/mL of IFN-β within HUVECs, control iPSECs, or patient iPSECs. HUVECs indicates human umbilical vein endothelial cells; IFN, interferon; iPSECs, induced pluripotent stem cell-derived vascular endothelial cells; MMD, moyamoya disease.

Values of $P<0.05$ were considered statistically significant. Statistical analyses were performed using SAS software (version 9.4; SAS Institute Inc., Cary, NC).

## Results

### Induction of RNF213 in HeLa Cells and HUVECs

We investigated the induction of RNF213 in HeLa cells and HUVECs after treatment of various angiogenic factors (TGF-β, IL-1β, VEGF, and PDGF-BB) and antiangiogenic factors (IFN-α, IFN-β, and IFN-γ). After 24 hours of treatment, none of the factors, except for IFN-γ, changed RNF213 protein levels in HeLa cells (Figure 3). However, IFN-γ increased RNF213 protein levels in a dose- and time-dependent manner (Figure 3A and 3B) with corresponding increases in mRNA levels (Figure 3C and 3D). We then investigated the effects of treatment with the same factors on HUVECs at the 24-hour time point. Whereas TGF-β, IL-1β, VEGF, and PDGF-BB did not change RNF213 protein levels (Figure 4A), IFN-β and IFN-γ, but not IFN-α, increased protein levels in a dose-dependent manner (Figure 5). IFN-β and IFN-γ also induced RNF213 in a time-dependent manner (Figure 4B and 4C). We further examined mRNA levels of *RNF213* after treatment with IFN-β and IFN-γ.

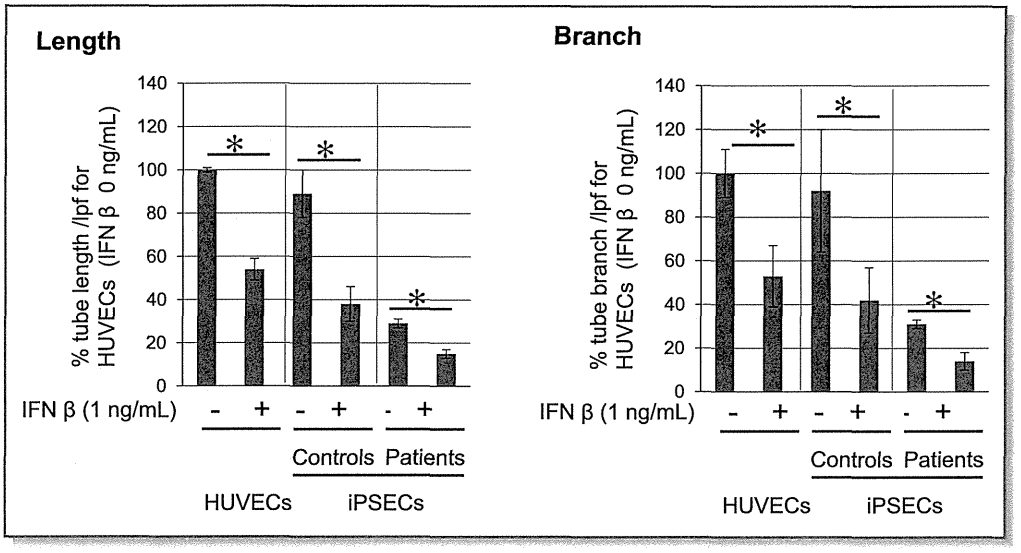


**Figure 14.** Tube formation assays for iPSECs after 20 hours of culture on Matrigel with IFN-β. HUVECs without IFN-β treatment served as the control (100%). Total tube length and number of branches were quantified by imaging analysis. A column with a bar represents mean±SD of 2 controls (blue) or 2 patients (red) in 3 independent experiments. *$P$<0.05, according to Student $t$ test comparing 0 ng/mL of IFN-β within HUVECs, control iPSECs, or patient iPSECs. HUVECs indicates human umbilical vein endothelial cells; IFN, interferon; iPSECs, induced pluripotent stem cell-derived vascular endothelial cells.

Both factors increased mRNA levels, but IFN-β increased mRNA levels at a lower dose (0.1 ng/mL) and an earlier time point (3 hours) than IFN-γ (Figure 4D through 4G).

These findings indicated that IFN-β increased *RNF213* expression levels in HUVECs in a vascular EC-specific manner, whereas IFN-γ did not. The other factors had no effect on expression levels of RNF213. Upregulation of RNF213 protein was preceded by an increase in RNF213 mRNA levels, which suggested that IFN-β increased *RNF213* expression at the transcriptional level. Because IFN-β induced RNF213 in HUVECs, we chose IFN-β for further characterization because of its tissue specificity.

## Induction of RNF213 by IFN-β Is Mediated by STATx

We examined the putative binding sites for transcriptional factors in the promoter region up to 3 kb from the transcriptional start site of the *RNF213* gene. We performed a computer search for potential regulatory elements in this region using MatInspector V2.2 at the TRANSFAC website (http://www.gene-regulation.com/pub/databases.html).[24] We found a single STATx-binding site at the −514 position (Figure 6A). STAT1 is a signaling molecule in the IFN-β-signaling pathway.[25,26] Therefore, we conducted promoter assays using a fusion plasmid containing the 3-kb *RNF213* promoter region and a luciferase reporter gene. The promoter significantly increased luciferase activity after treatment with IFN-β (Figure 6B), whereas disruption of the STATx-binding site by missense mutagenesis[27] abrogated promoter activity (Figure 6C). Therefore, we conclude that IFN-β upregulates RNF213 through the STATx-binding site in its promoter region.

## Role of RNF213 in Antiangiogenic Activity of IFN-β

First, we evaluated effects of treatment with IFN-β on HUVEC proliferation, and found that IFN-β did not increase proliferation (Figure 7). Angiogenic activity was then evaluated by tube formation and migration assays. We confirmed that IFN-β lowered tube formation and inhibited migration (Figures 8 and 9) without affecting proliferation rates (Figure 7). Because IFN-β induced RNF213, we hypothesized that antiangiogenic activity of IFN-β is mediated by RNF213. To test this hypothesis, we first depleted STAT1 by siRNA. Antiangiogenic activity of IFN-β, except for branching, was normalized by depletion of STAT1 and phosphorylated STAT1 by siRNA transfection (Figure 10A and 10B). Notably, siRNA also downregulated RNF213 (Figure 10A). This downregulation was likely mediated by activation of the promoter. We then depleted RNF213 protein levels by siRNA transfection. Depletion of RNF213 restored tube formation and migration (Figures 11 and 12). These rescue experiments by siRNA transfection demonstrated that RNF213 was involved in antiangiogenic activity of IFN-β in ECs.

## Effects of IFN-β on Angiogenic Activity of iPSECs

We then investigated effects of IFN-β treatment on tube formation by iPSECs derived from 2 control subjects with the

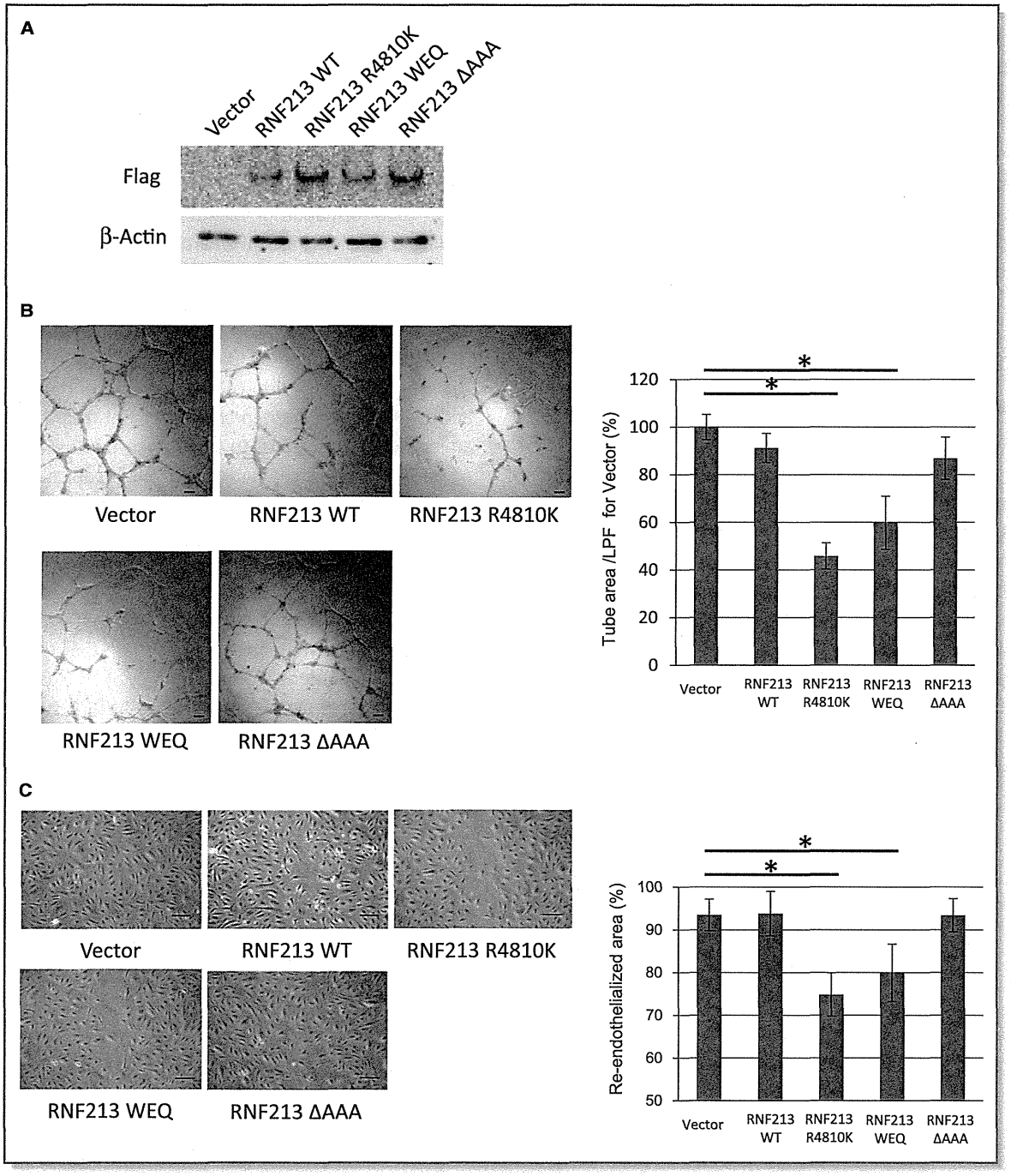


**Figure 15.** Angiogenic activity of RNF213 WT, and R4810K, WEQ, and ΔAAA mutants. A, RNF213 protein expression in HUVECs transiently expressing the RNF213 mutant. HUVECs transfected with the FLAG-RNF213 expression vector (RNF213 WT, RNF213 R4810K, RNF213 WEQ, and RNF213 ΔAAA) were immunoblotted using anti-FLAG antibodies. Empty vector ("vector" in the figure)-transfected HUVECs served as the control. Representative western blotting findings are shown. Similar results were obtained in 3 independent experiments. B, Tube formation assays for HUVECs transiently expressing RNF213 WT, RNF213 R4810K, RNF213 WEQ, and RNF213 ΔAAA. The vector served as the positive control (100%). Scale bars indicate 100 μm. Representative images are shown in left panel. Tube area was quantified by imaging analysis (right panel). A column with a bar represents mean±SD (n=3). **P*<0.05, according to Student *t* test compared with the vector. C, Migration assays for HUVECs transiently expressing RNF213 WT, RNF213 R4810K, RNF213 WEQ, and RNF213 ΔAAA. The vector served as the control. Scale bars indicate 100 μm. Representative images are shown in left panel. Re-endothelialized areas were quantified by imaging analysis (right panel). A column with a bar represents mean±SD (n=3). **P*<0.05 according to Student *t* test compared with the vector. HUVECs indicates human umbilical vein endothelial cells; LPF, low-pass filter; WEQ, Walker B motif; WT, wild-type.

WT RNF213 genotype and 2 MMD patients (homozygous for RNF213 R4810K). Treatment with IFN-β was accompanied by upregulation of RNF213 mRNA expression (Figure 13A). Notably, IFN-β treatment lowered tube formation in iPSECs in both of the control subjects and the MMD patients (Figures 13B and 14). These data support the notion that IFN-β treatment suppresses angiogenic activity in ECs with induction of RNF213 in humans. In the next step, we investigated the molecular mechanisms of antiangiogenic effects of RNF213.

## Loss of Function of the Walker B Motif in the First AAA$^+$ of RNF213 Lowers Angiogenic Activity Whereas a Deletion Mutation of the First AAA$^+$ Does Not Lower Angiogenic Activity

Mutation of glutamic acid of the Walker B motif (DExxbox) (WEQ) causes loss of function of ATPase hydrolysis.[28] The Walker B motif in the first AAA$^+$ of RNF213 is shown to stabilize hexamer formation, whereas deletion of the first AAA$^+$, which results in loss of ATPase activity, does not initiate oligomerization.[13] Therefore, we hypothesized that RNF213 WEQ mutation stabilizes oligomers and can cause deleterious effects in ECs by capture in the oligomeric state. We also hypothesized that RNF213 deletion of AAA$^+$, which does not allow formation of oligomers, does not result in any deleterious effects as silencing RNF213 in vitro[14] and in Rnf213 null mice.[14,17] Based on these hypotheses, we investigated the effects of expression of the vectors RNF213 WT, RNF213 R4810K, RNF213 WEQ, and RNF213 deletion of AAA$^+$ on tube formation and migration of HUVECs (Figure 15A). RNF213 WEQ decreased tube formation and migration, similar to RNF213 R4810K (Figure 15). In contrast, expression of RNF213 deletion of AAA$^+$ did not lower tube formation or migration, which is in accord with a finding that silencing RNF213 did not impair angiogenesis.[14] Expression of RNF213 WT did not decrease angiogenic activity. Therefore, we consider that RNF213 trapped in the oligomeric state may lead to low angiogenic activity.

We then investigated the effects of RNF213 R4810K on ATPase activity (Figure 16). Although we detected ATPase activity in Walker motif in a recombinant fragment containing amino acids from 2319 to 2613,[8] we had never determined ATPase activity with an entire 5207 amino acids. In the current study, we determined ATPase activity with the entire RNF213 proteins of WT, R4810K, and deletion AAA$^+$. Surprisingly, RNF213 R4810K resulted in a loss of ATPase activity. Under the present experimental conditions using excessive detergent washing, RNF213 protein may not be able to maintain an oligomeric form. Therefore, we postulate that the results may represent monomeric ATPase activity. RNF213 R4810K can form oligomers, similar to RNF213 WT,[13] suggesting that R4810K may stabilize oligomeric states of RNF213 by inhibiting ATP hydrolysis, thereby inhibiting ATPase activity.

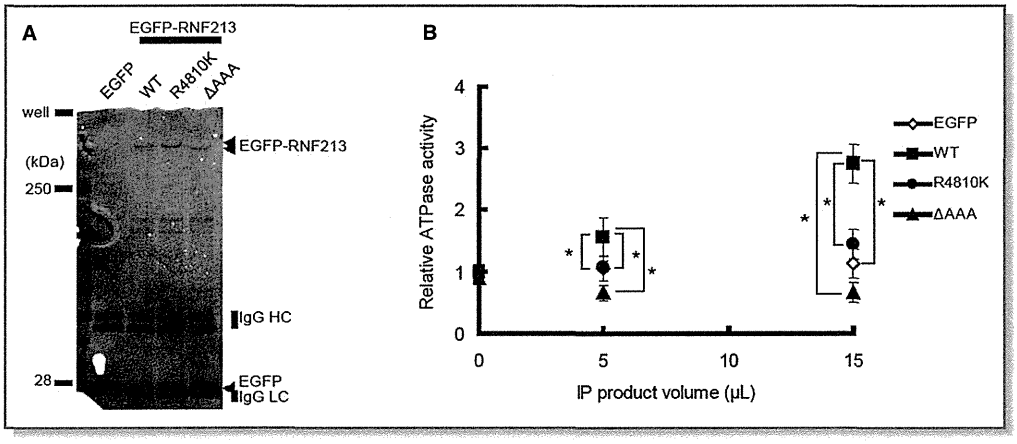


**Figure 16.** ATPase activity of RNF213 WT, R4810K, and ΔAAA mutants. A, Lysates from EGFP-RNF213–transfected HEK293 cells were IP with anti-GFP agarose. A total volume of 15 μL was subjected to SDS-PAGE followed by GelCode staining. RNF213 proteins fused with EGFP were detected in EGFP-RNF213–transfected cells (arrow heads, "EGFP-RNF213"). Representative SDS-PAGE images are shown. Similar results were obtained in 3 independent experiments. B, ATPase activity of immunoprecipitated extracts was assayed for ATPase activity. Indicated volumes (μL) of IP products were combined with buffer to yield a total volume of 50 μL for ATPase reaction for 30 minutes at room temperature (see details in the text). Phosphate release was measured using the Phosphate Sensor as ATPase activity. Relative activity was calculated based on average activity of EGFP at 0 μL, which was equal to 1. Data with bars represent mean±SD (n=3). *$P$<0.05 according to Student $t$ test compared with WT at 2 volumes. EGFP indicates enhanced green fluorescent proteins detected in EGFP-transfected cells (arrow head); IgG HC, IgG heavy chain; IgG LC, IgG light chain; IP, immunoprecipitated; Well, sample wells of the gel; WT, wild type.

## Effects of Expression of the RNF213 R4810K Ortholog Rnf213 R4757K on Cerebral Angiogenesis In Vivo

Our in vitro data strongly suggest that RNF213 R4810K lowers angiogenic activity in ECs when it is induced by environmental stimuli, such as IFNs. Therefore, we investigated the effects of ablation or upregulation of RNF213 R4810K in vivo using various genetically modified mice. These mouse strains involved ablation of Rnf213 (KO)[17] and Tg mice, which overexpresses Rnf213 (R4757K or WT) in ECs (EC: EC-Mut-Tg and EC-WT-Tg) or SMCs (SMC: SMC-Mu-Tg) (Figure 2). Tissue-specific upregulation of RNF213 was confirmed in Tg mice in ECs and SMCs (Figure 17). To induce cerebral angiogenesis, mice at 3 weeks of age were exposed to hypoxia (8% $O_2$ for 2 weeks). At the end of exposure, MRA was conducted in 3 mice for each strain. Exposure to hypoxia failed to induce angiogenesis in EC-Mut-Tg mice, whereas upregulation of Rnf213 WT in ECs, upregulation of Rnf213 R4757K in SMCs, and null Rnf213 or WT significantly induced angiogenesis (Figure 18). However, we could not find any stenotic lesions, moyamoya vessels, or lesions indicative of cerebral infarction in any mice with different genotypes (Figure 19).

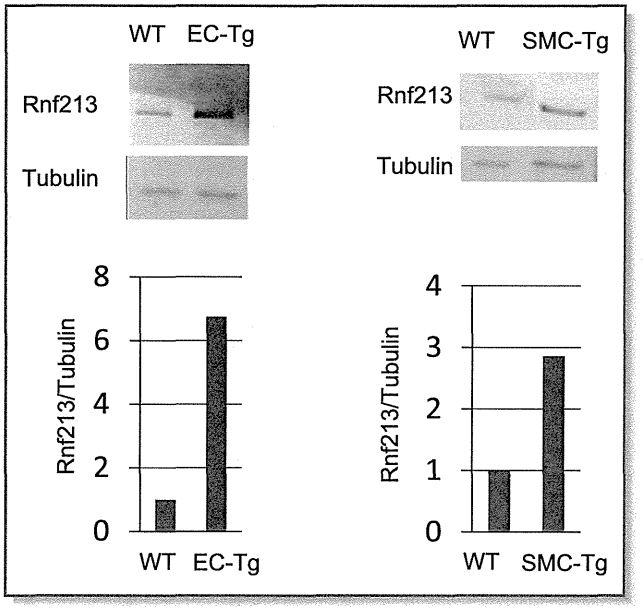


**Figure 17.** Tissue-specific upregulation of RNF213 in EC-Tg and SMC-Tg mice. Protein extraction from purified ECs from lungs of EC-Mut Tg and WT mice (left panel) and protein extraction from aorta of SMC-Mut Tg and WT mice (right panel) were immunoblotted. β-tubulin served as the loading control. Similar results were obtained from 3 independent experiments. ECs indicates endothelial cells; SMC, smooth muscle cells; Tg, transgenic; WT, wild type.

## Discussion

RNF213 is highly associated with MMD[9,29] and is a causative gene for MMD.[8] Although low angiogenesis has been reported with RNF213,[14] functional deviations caused by R4810K have not been investigated. Given that upregulation of R4810K may be important in development of MMD, the environmental stimuli that induce RNF213 remain unknown. Additionally, there are no animal models enabling to recapture the low-angiogenesis phenotype.

In the present study, we systemically investigated the effects of RNF213 R4810K on angiogenesis to address these issues discussed above. We found that upregulation could be produced by inflammatory signals of IFNs in HUVECs and ECs established from iPS cells from unaffected subjects and MMD patients. Upregulation of RNF213 by IFNs was consistently accompanied by lower angiogenesis, and silencing RNF213 partially ameliorated inhibition of angiogenesis by IFN-β. We also showed that upregulation of RNF213 was mediated by STATx in the promoter of the *RNF213* gene. These data collectively indicate that upregulation of RNF213 WT is causally associated with lower angiogenic activity after IFN-β exposure. Therefore, RNF213 is likely to be a mediator downstream of the IFN-β-signaling pathway in ECs that are primed by IFN-β in vivo. However, upregulation of RNF213 WT was not sufficient to elicit antiangiogenic signals independently, whereas upregulation of RNF213 R4810K was sufficient. This in vitro finding was further confirmed by the Tg animal model in hypoxia. RNF213 R4757K (R4810K ortholog) inhibited angiogenesis in mice that overexpressed RNF213 in ECs. However, none of the mice with upregulation of the WT in ECs, upregulation of R4757K in SMCs, or null Rnf213 inhibited angiogenesis. Taken together, these data indicate that RNF213 R4810K can inhibit angiogenesis under conditions of exposure to IFNs or hypoxia, whereas RNF213 WT can only inhibit angiogenesis in the IFN-signaling pathway. It should be addressed that the current study clearly demonstrated the primary role of ECs in angiogenesis. This finding demonstrated a sharp contrast, with an anticipation that SMCs plays a critical role in the development of vascular remodeling. Collectively, we successfully demonstrated substantial roles of RNF213 R4810K in the low-angiogenesis phenotype in response to environmental stimuli. However, the issue of whether known functional impairment (ie, inhibition of cellular proliferation[14] or mitotic abnormalities[15]) associated with RNF213 R4810K is involved in reduced angiogenesis after hypoxia in EC-specific RNF213 R4757K Tg mice needs to be examined in the future.

The current results suggest that carriers of RNF213 R4810K may be susceptible to cerebral hypoxia because of insufficient angiogenesis if inflammation and hypoxia simultaneously occur. These IFNs are induced by viral and bacterial infections and are upregulated in autoimmune patients, who are often complicated

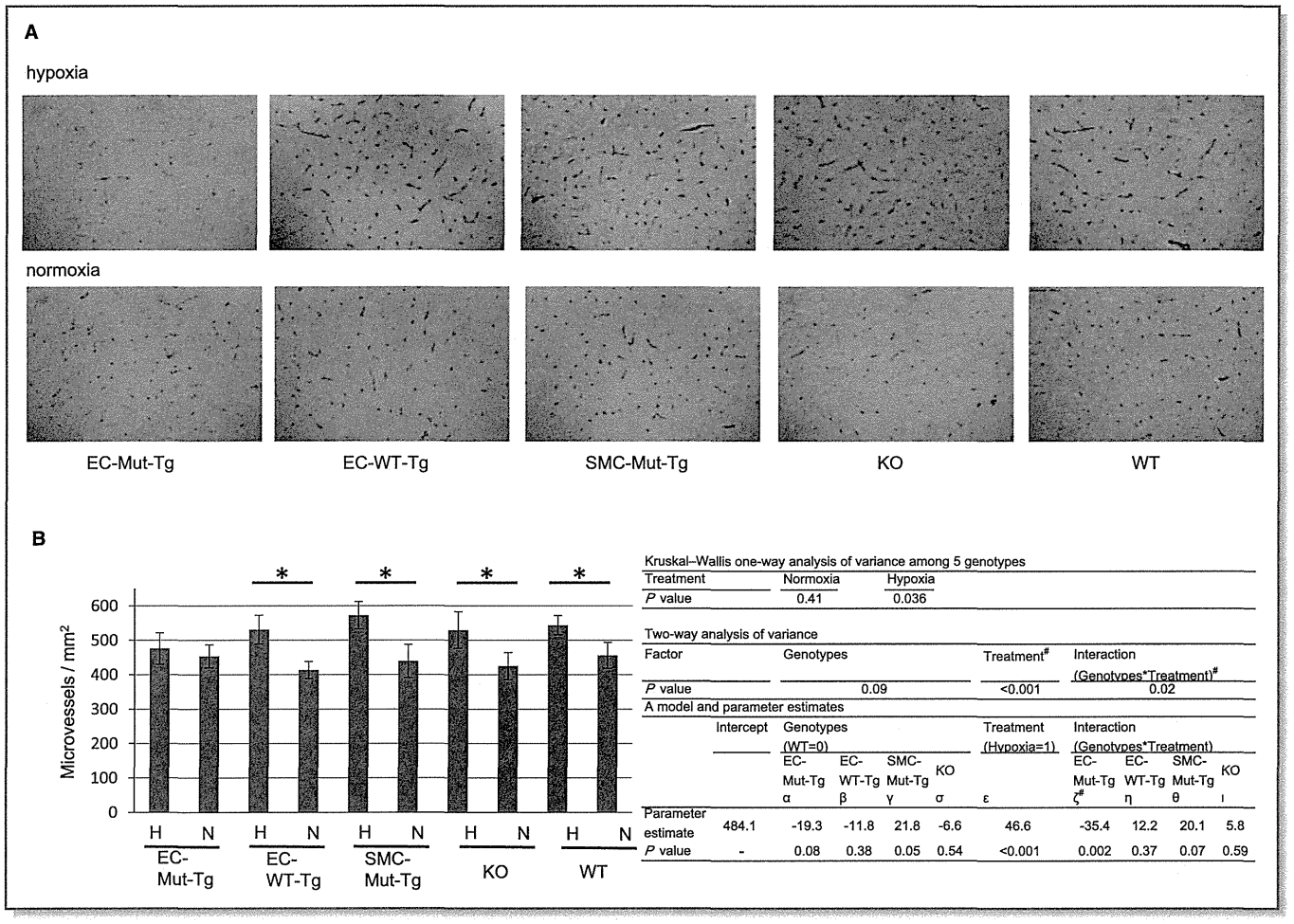


Kruskal–Wallis one-way analysis of variance among 5 genotypes

| Treatment | Normoxia | Hypoxia |
|---|---|---|
| *P* value | 0.41 | 0.036 |

Two-way analysis of variance

| Factor | Genotypes | Treatment# | Interaction (Genotypes*Treatment)# |
|---|---|---|---|
| *P* value | 0.09 | <0.001 | 0.02 |

A model and parameter estimates

| | Intercept | Genotypes (WT=0) | | | | Treatment (Hypoxia=1) | Interaction (Genotypes*Treatment) | | | |
|---|---|---|---|---|---|---|---|---|---|---|
| | | EC-Mut-Tg α | EC-WT-Tg β | SMC-Mut-Tg γ | KO σ | ε | EC-Mut-Tg ζ# | EC-WT-Tg η | SMC-Mut-Tg θ | KO ι |
| Parameter estimate | 484.1 | -19.3 | -11.8 | 21.8 | -6.6 | 46.6 | -35.4 | 12.2 | 20.1 | 5.8 |
| *P* value | - | 0.08 | 0.38 | 0.05 | 0.54 | <0.001 | 0.002 | 0.37 | 0.07 | 0.59 |

**Figure 18.** Suppressive effect of Rnf213 mutant upregulation in ECs on angiogenesis in vivo. A, Representative images of GLUT-1-stained sections of cerebral cortex of EC-Mut Tg, EC-WT Tg, SMC-Mut Tg, KO, and WT mice under conditions of normoxia (N) and hypoxia (H). B, Quantified result of cerebral microvessels (left panel). A column with a bar represents mean±SD of the number of cerebral microvessels/mm$^2$ *from 6 mice per group. In the hypoxia condition, there was a significant difference in the number of cerebral microvessels among 5 genotypes* using the nonparametric method, Kruskal–Wallis 1-way ANOVA ($P$=0.036), but not in the normoxia condition ($P$=0.41). *$P$<0.05 according to Mann–Whitney *U* test compared with normoxia condition. Two-way ANOVA method was conducted for microvessel formation between genotypes and treatment with interaction term. Results and parameter estimates are described in table (right panel). Regression models are described as (microvessels)=(intercept)+α×[Genotype: EC-Mut-Tg]+β×[Genotype: EC-WT-Tg]+γ×[Genotype: SMC-Mut-Tg]+δ×[Genotype: KO]+ε×[Treatment]+ζ×[interaction: EC-Mut-Tg]+η×[interaction: EC-WT-Tg]+θ×[interaction: SMC-Mut-Tg]+ι×[interaction: KO]. Treatment (hypoxia) significantly induced the number of microvessels/mm$^2$ ($P$<0.001), whereas genotype did not ($P$=0.09). Interaction between genotype and treatment was significant ($P$=0.02). The coefficient on EC-Mut-Tg (ζ) was negative, suggesting that this genotype did not increase microvessels ($P$=0.002). #$P$<0.05 according to 2-way ANOVA. ECs indicates endothelial cells; GLUT-1, glucose transporter; KO, knockout; SMC, smooth muscle cells; Tg, transgenic; WT, wild type.

by encephalitis.[30] Our study may imply that IFNs initially play a major role and are causally associated with insufficient angiogenesis in infectious or autoimmune diseases with MMD, as observed in accumulated clinical cases of MMD.[31]

In the present study, we found that a mutation in the AAA$^+$ module toward stabilization of oligomers is responsible for a low-angiogenesis phenotype. We showed that the Walker B motif in the first AAA$^+$ module of RNF213 had an inhibitory effect on angiogenesis. In contrast, deletion of the first AAA$^+$ module did not have any discernible effects on angiogenesis. Intriguingly, both mutations resulted in loss of ATPase activity, but the WEQ mutation resulted in stabilization of oligomers, whereas deletion of AAA$^+$ did not result in oligomerization. If this is the case, RNF213 R4810K, which decreased angiogenic activity and resulted in loss of ATPase activity in our study, may stabilize oligomers once they are formed and thus impair angiogenesis, suggesting a dominant negative mechanism. Furthermore, absence of a discernible effect of upregulation of deletion of the first AAA$^+$ RNF213 on angiogenesis is in agreement with an observation in RNF213 null mice in which angiogenesis was not inhibited in the brain after exposure to hypoxia. Collectively, the current